13

UNCONVENTIONAL PATTERNING METHODS FOR BIONEMS

Pilnam Kim, Du Yanan, Ali Khademhosseini,
Robert Langer, and Kahp Y. Suh

13.1 INTRODUCTION

Unconventional nanopatterning methods are emerging as powerful tools for biological studies and tissue engineering [1–5]. In biological studies, there is a great need to detect or separate small biological species (DNA or proteins) in a rapid and high throughput manner. Most biological events occur at the nanometer scale and thus control of the phenomena at this characteristic length scale could lead to new devices with improved properties such as increased speed and sensitivity. Nanoscale patterns or channels integrated with bio-nanoelectromechanical systems (BioNEMS) enable miniaturization of biomolecular arrays or detection elements, offering a potential tool for screening libraries of small molecules or detection/separation at a single molecule level [6]. In tissue engineering, it is important to control cellular microenvironments *in vitro* to create the cellular niche during embryonic development. For this purpose, unconventional patterning methods can offer biomimetic nanoscale topographical features on a solid substrate similar to tissue environments, providing a route to manipulate cell functions with desired phenotypic responses.

In a typical biological laboratory setup, it is beneficial to create nanoscale patterns or nanochannels without resorting to sophisticated equipments such in electron-beam, x-ray, and ultraviolet (UV) photolithography. Nanoimprinting (including hot

Unconventional Nanopatterning Techniques and Applications by Hong H. Lee and John A. Rogers

embossing and UV-assisted imprinting) or soft lithographies are low cost and flexible patterning techniques, capable of fabricating polymeric structures for biological applications. Currently, established silicon and glass processes show limitations due to complex fabrication procedures, geometrical design restrictions, and high costs involved. The need for high aspect ratio features for various biological and biomedical applications also posed a serious problem to the existing nanofabrication technologies in silicon and glass. Polymers offer a solution to these challenges and enable mass fabrication of biomolecular arrays or nanofluidic devices. In addition, polymers offer several advantages that are not readily available in silicon and glass, including a wide range of material characteristics, biological compatibility, ease of processing and prototyping, and lower costs.

In this chapter, we focus on simple replication technologies for polymers (contact printing, nanoimprint lithography, nanomolding, soft lithography, etc.) that have been used to create nanoscale channels, patterns, or topographies for biological studies and tissue engineering.

13.2 FABRICATION OF NANOFLUIDIC SYSTEM FOR BIOLOGICAL APPLICATIONS

Microfluidic devices have been a well-established microscale technology in biological applications for manipulating small quantities of sample in a fast, high resolution, and low cost manner. As devices continue to scale down to the nanometer dimension, there has been a growing interest in nanofluidics, which offers the possibility for single-molecule manipulation [7]. Nanochannel, as the most commonly used configuration for nanofluidic systems, is defined as nanofabricated channels with at least one cross-section dimension on the nanometer scale (one dimensional (1D) and two dimensional (2D) nanochannels) [8]. The nanoscale dimensions of the nanochannel can be comparable to the size of the fluid macromolecules such as proteins and DNA, and a significant amount of the fluid in the nanochannel is in contact with the channel surface leading to significant increase in the effects of surface forces [9]. These unique fluidic properties offer new opportunities to investigate new fundamental phenomena (i.e., fluidic transport and molecular behavior) and develop tools for biomedical applications [10–12].

Here, we introduce several fabrication strategies of nanochannels with the emphasis on unconventional fabrication methods, including nanoimprinting, nanomolding, and soft lithography. We then discuss several exemplified biomedical applications of the nanochannels system including DNA sequencing/stretching, protein separation, and drug delivery.

13.2.1 Unconventional Methods for Fabrication of Nanochannel

Conventional microfabrication methods have been used to fabricate nanochannels in substrate (wafer or film) by standard photolithography patterning followed by wet–dry substrate etching. For standard photolithography patterning, a beam of UV

light passes through a mask and lens, which can create nanochannel patterns with the resolution of sub-100 nm [13, 14]. Higher resolution of the patterning can be achieved by using extreme UV light [15, 16] to create narrower nanochannels. Also, lithography technologies based on focused beams such as electron-beam lithography (EBL) [7, 17] and focused ion beam (FIB) lithography [18, 19] are attractive alternatives to create highly precise and reliable nanochannel patterns with features without using the mask. Other maskless patterning methods for nanochannels fabrication include interferometric lithography (IL) (based on the interference of two and more coherent beams) [20], laser patterning [21, 22] and surface machining (by etching of the nanometer height sacrificial layer) [23].

Here, several exemplary works of applying unconventional patterning methods are listed for nanochannel fabrication. All these unconventional patterning methods can be used to fabricate nanochannels using functional materials other than photoresist with sub-100-nm resolution and the fabrication processes are fast and low cost without extensive use of "clean rooms" and photolithographic equipment [24].

13.2.1.1 Nanochannel Fabrication by Nanoimprint Lithography (NIL).

NIL and NIL-related techniques, such as step-and-flash imprint lithography (S-FIL) can be used as a low cost, high throughput method for the fabrication of nanochannels.

Abgrall et al. [25] applied NIL to fabricate planar low aseptic ratio (AR) nanochannels with width in micrometer scale and depth under 100 nm. (Figure 13.1*a*). First, a silicon mold with the impression of nanochannel was fabricated using standard photolithography and reactive ion etching (RIE). Next, a layer of poly(methylmethacrylate) (PMMA) was hot embossed by this silicon mold to create the nanochannels in PMMA. Subsequently, a second layer of PMMA was bonded to the first sheet by thermal bonding for sealing of the nanochannels. They have successfully fabricated arrays of sealed planar nanochannels in PMMA with a depth of 80 nm and low AR ranging from 0.008 to 0.05. Q1

Cao et al. [26] made uniform arrays of nanochannels over large areas of ∼100-mm silicon wafer using NIL (Figure 13.1*b*). The NIL mold was generated by IL. The nanochannels were further narrowed and sealed by techniques that are based on nonuniform deposition (electron-beam deposition and sputter deposition). The resulting sealed channels had a cross-section as small as 10 nm by 50 nm. The same NIL technique has also been applied to build a sealed 100-nm wide, 200-nm deep nanochannel array on fused silica wafers (Figure 13.1*c*) [27].

Wang et al. [28] present results on fabrication of high density nanochannels in SU-8 resist, based on nanoimprinting combined with UV curing (S-FIL) (Figure 13.1*d*). Silicon template with nanopatterns was fabricated by EBL and RIE. A thick layer of SU-8 was spin coated onto a quartz wafer, imprinted by the template, and exposed to UV light through the quartz substrate for curing. Finally, the template was removed to obtain the SU-8 nanochannel. Due to the low viscosity of the SU-8, large-area patterns with high resolution, high density, high uniformity, and high aspect ratio could be replicated under low pressure and low temperature.

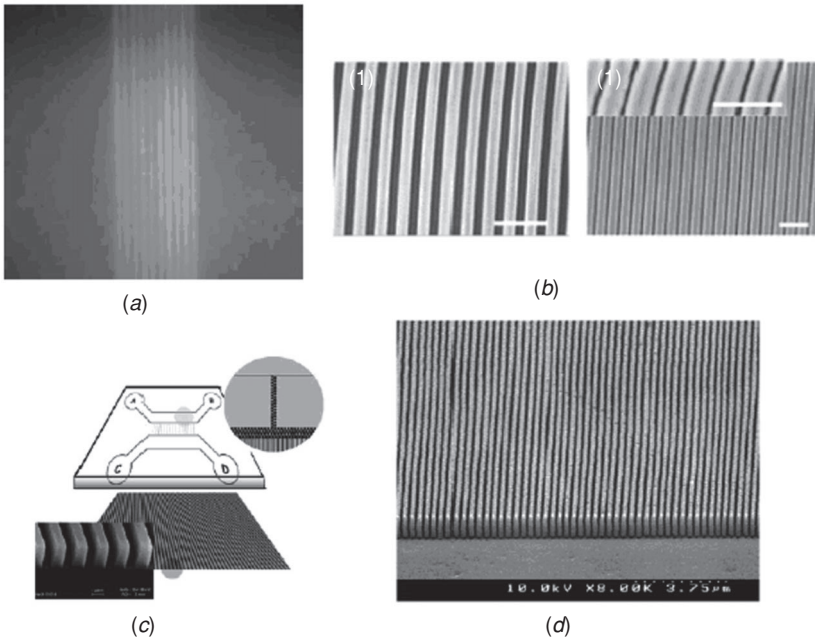

Figure 13.1. Nanochannel fabrication by NIL. (*a*) Planar PMMA nanochannels with a width of 10 μm and a depth of 80 nm filled with fluorescent dye. (Reprinted with permission from [25] and the Royal Society of Chemistry.) (*b*) Nanochannels in silicon wafer with a trench width of 85 nm. (1) The dark area is the trench. (2) The channels were narrowed down to less than 20 nm by controlled electron-beam deposition. The inset shows the channel width at a higher magnification. The scale bars are all 500 nm. (Reprinted with permission from [26] and the American Institute of Physics.) (*c*) The assembly of a sealed 100-nm-wide, 200-nm-deep nanochannel array with a microfabricated coverslip. The nanoimprinted chips were made in fused silica (thickness, 1 mm). (Reprinted with permission from [27] and the National Academy of Sciences.) (*d*) High density nanochannels in SU-8 fabricated by S-FIL, the pitch, the height, and the linewidth of nanochannels were 300, 850, and 150 nm, respectively with high aspect ratios of 5–6. (Reprinted with permission from [28] and the Elsevier B.V.)

13.2.1.2 Nanochannel Fabrication by Nanomolding. In principle, nanomolding techniques use a mold in the inverse shape of the desired nanostructures, which is filled with a structural material and then the mold can be etched or removed leaving the desired structure behind [13]. Common nanomolding techniques are based on micromolding in capillaries (MIMIC), solvent-assisted micromolding (SAMIM) [24], and capillary force lithography (CFL). In MIMIC, structures are filled with a thermal or photocurable, low viscosity liquid (i.e., prepolymer or hydrogel) by capillary force. When the stamp is removed, the patterned structure is left on the substrate. In SAMIM, the surface of the mold is wetted with a solvent and pressed against the polymer film at ambient conditions. The solvent softens the polymer and as the solvent evaporates, the polymer conforms to the nanostructure of mold. SAMIM enables molding of polymers that cannot be

implemented with S-FIL or NIL. In CFL, a patterned elastomeric mold is placed on a spin coated polymer film (thermoplastic or UV-curable resin), followed either by raising temperature above the polymer's glass transition temperature (T_g) or by direct molding prior to solvent evaporation, or by exposing UV light to solidity the precursor film.

Kim et al. [29] presented a simple, yet robust method for fabricating PEG-based nanochannels by CFL. As illustrated in Figure 13.2*a*, a UV-curable poly(ethylene glycol) (PEG) polymer such as PEG dimethacrylate (PEG-DMA) or PEG diacrylate (PEG-DA) was drop dispensed on photolithography-fabricated silicon master and a supporting poly(ethylene terephthalate) film was carefully placed on top of the polymer surface to make conformal contact. To cure, the sample was exposed to UV for a few seconds (PEG-DA) to a few tens of seconds (PEG-DMA). A slight physical pressure was applied to make conformal contact. With additional UV exposure, irreversible bonding occurred through photo-induced cross-linking at the interface. This method was used to form channels as small as 50 nm in diameter without using a sophisticated experimental setup. Recently, the same group used the UV-curable PEG-DA as a mold to form reversibly bonded nanocapillaries (with a resolution of 50 nm on a gold or silicon substrate [33].

Lensen et al. [30] built nanochannel patterns in the bulk of the star PEG hydrogel by a UV-based imprinting with a perfluorinated soft mold. As illustrated in Figure 13.2*b*, a primary (hard) master was fabricated by photo- or electron-beam lithography. This primary master was replicated by the perfluorinated polyether (PFPE) material by means of UV curing of the prepolymer against the mold, resulting in an elastic, secondary master. The elasticity and the low surface energy of this PFPE material was easily peeled off mechanically and then used as a mold to imprint the structure into the UV-curable star PEG material. This method is a fast and simple technique with sub-100-nm resolution in dimension, which can be carried out on the bench top.

Lee et al. fabricated nanochannel patterns in poly(4-vinylpyridine) (P4VP) via SAMIM using a blending of two UV-curable materials, Norland Optical Adhesives (NOA) 63 and PEG-DA, in an appropriate ratio. Physical nanopatterning via the SAMIM process was carried out as shown in Figure 13.2*c*. A layer of P4VP solution, dissolved in ethanol, was spin coated on a Si wafer treated with oxygen plasma and the P4VP film was heated on a hot plate to evaporate the residual ethanol in the coated P4VP film. The composite mold was soaked in ethanol followed by drying by blowing with air. The composite mold was brought into conformal contact with the P4VP-coated Si wafer under mild heating to complete the SAMIM [31].

Another type of mold machining for fabricating nanochannels was reported by Ilic et al. [32]. The authors described a fabrication method for forming self-sealing parylene polymer tubes by depositing parylene polymer on the silicon wafer mold etched with nanochannel patterns (Figure 13.2*d*). The parylene polymer is chemically inert and biocompatible. Tubes were self-sealed as the parylene polymer "pinches off" during the deposition process to leave closed tubes with sub-micrometer lateral dimensions.

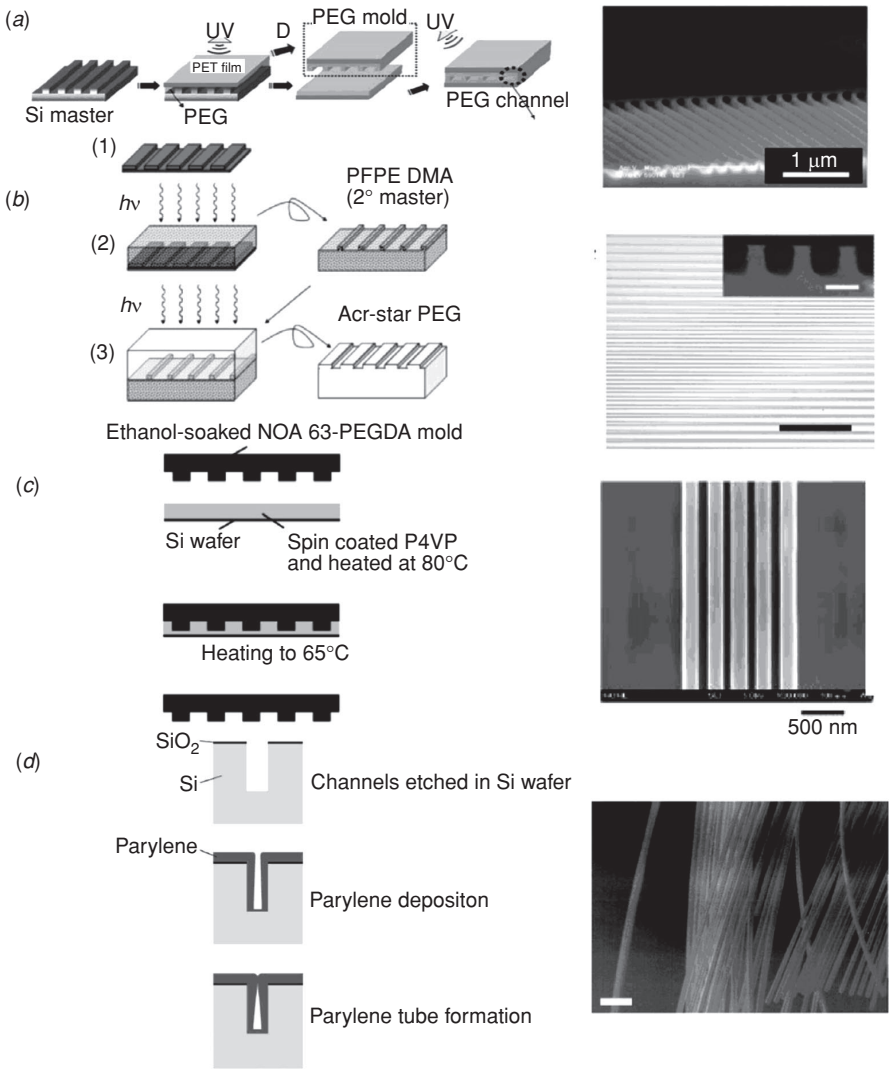

Figure 13.2. Nanochannel fabrication by nanomolding. (*a*) Left: schematic illustration of the experimental procedure for nanochannel fabrication; right: cross-sectional SEM images of various PEG channels with width of 50 nm (Reprinted with permission from [29] and the Royal Society of Chemistry.) (*b*) Left: schematic representation of the three-step process to structure bulk star PEG material; right: optical micrographs of replicas formed by Acr-star PEG using a PFPE secondary master, scale bar represents 100 μm. Insets (scale bar represents 10 μm). (Reprinted with permission from [30] and the American Chemical Society.) (*c*) Left: schematic illustrations for physical patterning of P4VP via SAMIM; right: SEM images of P4VP nanochannel on a Si wafer. (Reprinted with permission from [31] and the American Chemical Society.) (*d*) Left: schematic illustration of the self-sealed parylene tube formation (Reprinted with permission from [13] and the Royal Society of Chemistry); right: array of freely suspended parylene tubes. Scale bar corresponds to 5 mm. (Reprinted with permission from [32] and the AVS Science and Technology of Materials, Interfaces, and Processing.)

13.2.1.3 Nanochannel Fabrication by Soft Lithography. Soft lithography broadly refers to molding, embossing, and imprinting methods exclusively using an elastomeric mold and/or stamp such as poly(dimethylsiloxane) (PDMS) [24]. PDMS has been widely applied for nanochannel fabrication.

Kovarik et al. fabricated PDMS nanochannel with 130 nm deep and 580 nm wide (Figure 13.3*a*) [9]. The authors used EBL to form nanochannel masters in SU-8.

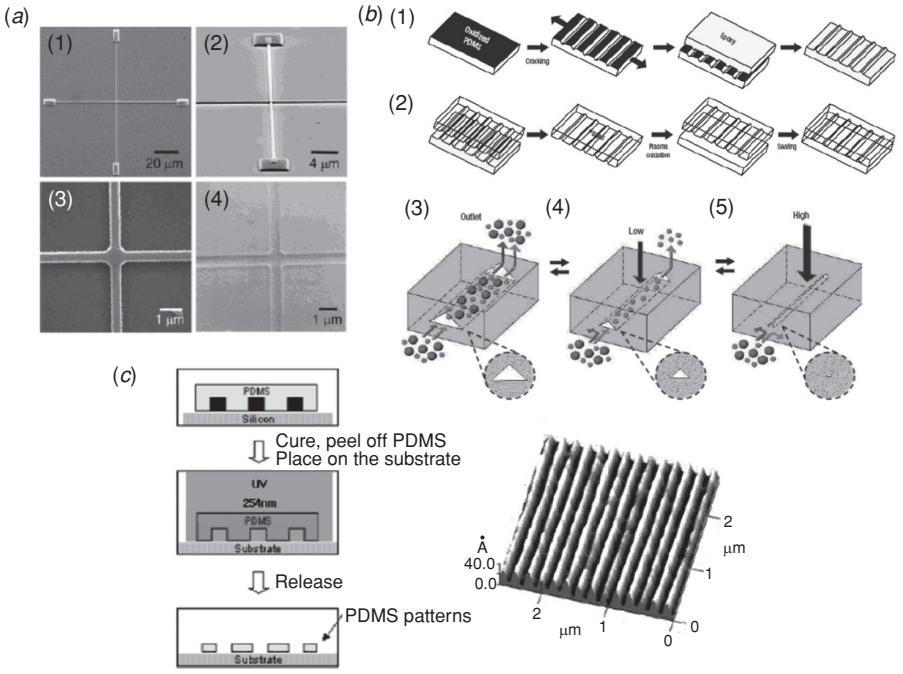

Figure 13.3. Nanochannel fabrication by soft lithography. (*a*): (1) SEM image of a cross-channel master fabricated in SU-8, (2) image of the same master taken at an 81° tilt, (3) enlarged view of the intersection of the channel mold, (4) image of the cross-intersection on a PDMS replica of the master seen in parts (1)–(3). Replica channels were 130 ± 10 nm deep and had an average width of 580 ± 40 nm. (Reprinted with permission from [9] the American Chemical Society.) (*b*) Fabrication of structurally stable elastomeric nanochannels. (1) A PDMS slab exposed to oxygen plasma is stretched to generate linear nanoscale cracks. The nanocracks are replicated onto ultraviolet-curable epoxy. (2) PDMS prepolymer is cast against the epoxy mold to generate negative relief patterns of nanochannels. The PDMS substrate is then briefly oxidized and sealed against an oxidized PDMS slab to form an array of enclosed nanochannel. (3)–(5) The mode of transport with different size selectivity can be switched reversibly by changing the magnitude of applied force (3): the larger nanochannels allows both larger and smaller particles to pass through simultaneously; (4) low levels of compressive stress constrict the channel such that only the smaller particles pass through; (5) nanochannels loaded with larger stresses become extremely small, excluding sample particles regardless of their size. (Reprinted with permission from [34] and the Nature Publishing Group.) (*c*) Left: schematic illustration of fabricating patterned PDMS by LSL; right: atomic force microscopy images of the nanochannel patterns of PDMS fabricated by LSL in silicon substrate. (Reprinted with permission from [35] and the American Chemical Society.)

The mixture of PDMS prepolymer and curing agent was then poured over the SU-8 master for molding and released to form the nanochannel.

A tunable-oxidized PDMS nanochannel was fabricated by Huh et al. [34], which could actively manipulate nanofluidic transport through dynamic modulation of the channel cross-section using remarkably small forces. As illustrated in Figure 13.3*b*, the PDMS nanochannels could be easily fabricated and provide a remarkably versatile example of an active nanostructure that can change its architecture during operation to create, control, and manipulate various types of nanofluidic transport.

Park et al. [35] reported a new soft lithography patterning method, called light-stamping lithography (LSL), that uses UV-induced adhesion of PDMS to fabricate PDMS nanochannels (Figure 13.3*c*). First, a patterned PDMS stamp was fabricated and brought into contact with a substrate surface. Second, the substrate was exposed through the PDMS stamp to a 254-nm UV lamp for 2 min. The UV light induced the formation of chemical bonds between the PDMS stamp and the substrate underneath. Finally, the PDMS stamp was physically peeled off from the substrate, with remaining torn pieces thereon.

In this section, we have listed examples of the use of unconventional methods for nanochannel fabrication. Several points need to be taken into consideration when designing a nanochannel. First, there exists a critical dimension of nanochannels before collapse due to the competition between van der Waals forces and the stiffness of the nanochannel material. The maximal width of a channel with a depth of 100 nm is around 70 nm PDMS and 170 nm for PMMA, indicating that the fabrication of high AR nanostructures in soft materials is not achievable [25]. Second, the bonding of the nanochannels is challenging due to the low AR. Great care should be taken when choosing the bonding methods, such as adhesive bonding, microwave bonding, solvent-assisted bonding, oxygen plasma-assisted bonding, and thermal bonding.

13.2.2 Application of Nanofluidic System

Nanochannels, having dimensions comparable to the size of biological macromolecules such as proteins and DNA, have attracted attention in biological applications. New phenomena arise with transition from microfluidics to nanofluidics as the typical dimension is reduced to below 100 nm. As the volume of fluid inside the channel becomes smaller, the quantity of surface charge becomes comparable to the quantity of bulk charge leading to co-ion exclusion and a surface-charge-governed regime of ion transport [25]. The confinement of biomolecules such as DNA or proteins in these structures allows applications, such as single-molecule manipulation/detection, bio-separation, and controlled drug delivery.

13.2.2.1 DNA Stretching and Sequencing. The ability to stretch single DNA molecules can be used for many biological applications, i.e., in DNA sequencing and in the study of DNA–protein interaction. In shotgun DNA sequencing, the location of landmark restriction sites on chromosomal length DNA molecules is a powerful method to ensure the faithful representation of the assembled DNA sequences to the native genome [36]. The restriction sites can be determined by gel electrophoresis

[37] or alternatively by optical mapping of the stretched DNA molecules [27]. DNA stretching is imperative to guarantee one-to-one mapping between the spatial position along the DNA molecules and position within the genome by using optical techniques directly [38]. Studies of DNA–protein interaction at the single molecule level are increasingly used to quantify distributions of molecular mechanical properties, transient intermediates, and reaction pathways [39], which require stretching and immobilization of DNA molecules to suppress Brownian motion, so that protein motion along the DNA contour can be followed.

Stretching of DNA trapped on a surface has been realized by several strategies, for example: (i) stretching by force exerted by a receding air–water interface on a hydrophobic surface (molecular combing) [40], (ii) stretching with optical or magnetic tweezers, laminar flows, atomic force cantilevers, or electric fields [41], or (iii) confinement stretching in the nanochannels [27]. Stretching DNA in the nanochannels has several advantages over other techniques: (i) external force is not required, because a long DNA molecule tends to spontaneously elongate and enter nanochannels directly from the environment due to the large free energy needed to reduce entropy, (ii) continuous measurement of the entire length of the DNA can be achieved due to the alignment of the elongated DNA molecular confine in the nanochannels.

Wang et al. [18] have fabricated open nanofluidic channel arrays in a Si3N4 membrane surface using the FIB milling technique for DNA stretching. Fluorescently stained λ-DNA molecules were put inside the nanochannels by capillary force and were stretched and transferred along these nanochannels (Figure 13.4*a*). Mannion et al. [42] have used the interface between a nanochannel and a microchannel as a tool for applying controlled forces on a DNA molecule. The entropic force was used to stretch molecules, to retract molecules from the nanochannels, and to straighten folded strands. Tegenfeldt et al. [27] used a 100-nm nanochannel array for DNA stretching and measured directly the contour lengths of a single DNA molecule confined in the channels. Dukkipati et al. have developed a novel DNA stretching method named "protein-assisted DNA immobilization," which utilizes the specific interactions between the DNA and DNA-binding proteins and evaporation-driven flow inside the microchannel. In this approach, the DNA–protein complex was first stretched out when subjected to an evaporation-driven hydrodynamic flow inside a microchannel, and then was immobilized onto the surface of the microchannel by the physical absorption of the protein part of the DNA–protein complex (Figure 13.4*b*) [39].

Cao et al. [26] have fabricated arrays of millions of nanochannels over a 100-mm wafer using nanoimprinting lithography to stretch, align, and analyze long genomic DNA in a highly parallel fashion. The same group also attempted to overcome the difficulties to introduce long genomic DNA molecules into nanometer scale fluidic channels directly from the macroscale world due to the steep entropic barrier. They designed continuous spatial gradient structures, which smoothly narrow the cross-section of a volume from the micro to the nanometer length scale and greatly reduce the local entropic barrier to the nanochannel entry (Figure 13.5) [43].

Several concerns may be considered when applying nanochannel for DNA stretching: (1) the dimensions of nanofluidic structures are critical for uniformly

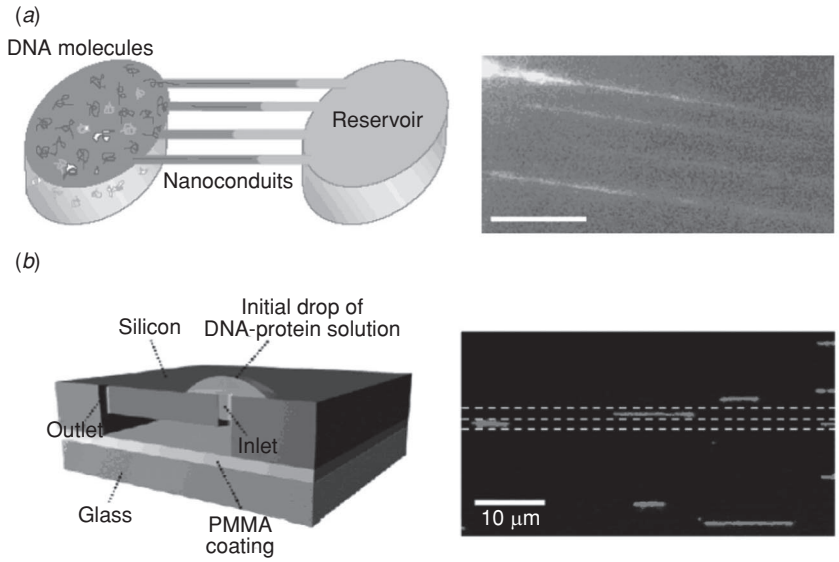

Figure 13.4. Examples of DNA stretching in the nanochannels. (*a*) Left: stained DNA molecules were put inside sub-100-nm conduits by capillary force and were stretched and transferred along these conduits; right: fluorescent images of the stretched DNA. (Reprinted with permission from [18] and the IEEE.) (*b*) Left: schematic diagram of the nanofluidic channels to immobilize and stretch DNA; right: fluorescent image of stretched DNA. (Reprinted with permission from [39] and the American Chemical Society.)

stretching long DNA; usually the width of the nanochannels should be smaller than the persistence length of double stranded DNA (∼50–70 nm) [44]. (2) Besides introducing the DNA molecules into the nanochannels spontaneously by passive transport (i.e., capillary force), positive transport of the DNA molecule into the nanochannels can be achieved by electrokinetic-driven or pressure-driven transport [45].

13.2.2.2 Protein Separation. Micro/nanofluidic separation systems have generated much interest as an enabling technology for processing complex protein samples. Decreasing the sample complexity by separation is crucial for increasing sensitivity of downstream detection tools for proteomic studies. This is required since most biomolecule detection tools (such as mass spectrometry and antibody-based biosensors) have a limited dynamic range of detection, while complex samples such as blood usually contains more than 10,000 different protein species with concentrations that vary up to nine orders of magnitude. Compared with conventional protein separation tools, such as nanoporous gels or membranes, micro/nano fluidic separation systems do not use any buffer additive or matrix, which facilitates their integration into the standard MEMS processes. These devices are mechanically and chemically more robust and could be precisely engineered to have better separation efficiencies.

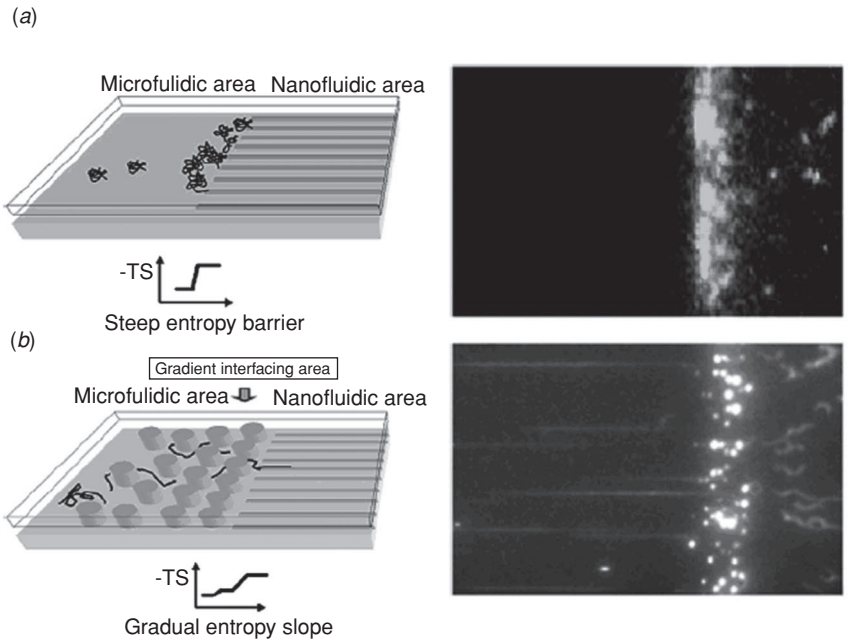

Figure 13.5. An improved nanochannels system for DNA stretching. (*a*) Left: schematic diagram showing regular nanofluidic channels; right: fluorescent images of long DNA molecules congregating at the edge of the regular nanofluidic chip without entering the normal nanochannels. (*b*) Nanochannels with continuous spatial gradient structures. Partially stretched long DNA molecules in the micro-post array and the gradient zone continuously entering the nanochannels in the left and being fully stretched. (Reprinted with permission from [43] the American Institute of Physics.)

Various attempts have been made at fabricating nanofluidic-based protein separation devices. For example, Han et al. separated proteins that were smaller than the gap size of the nanofluidic channel using steric hindrance effect of the biomolecules (Figure 13.6) [46]. They fabricated nanofluidic filter devices (nanochannels with gaps) on silicon substrate by standard photolithography and etching techniques. Protein separation was achieved by the free energy barrier introduced by the nanofluidic filter, since the entropy of protein has to be decreased in order to enter the nanofluidic filter. SDS-coated proteins have been successfully separated in a nanofluidic channel that has the filter gap thickness between 60 and 120 nm. Wang et al. [47] have developed a micro/nano fluidic sample concentration system based on electrokinetic trapping and nonlinear electro-osmotic flow. The separation device generated ion depletion (resulted by the net transfer of the charges between the anode and cathode), which induced electrical double layer within micro/nano channels. The electrical double layer was used to both collect and trap the molecules efficiently. A rapid preconcentration of proteins and peptides was achieved up to 10^6–10^8 fold in concentration, without using any physical barriers or reagents. Q2

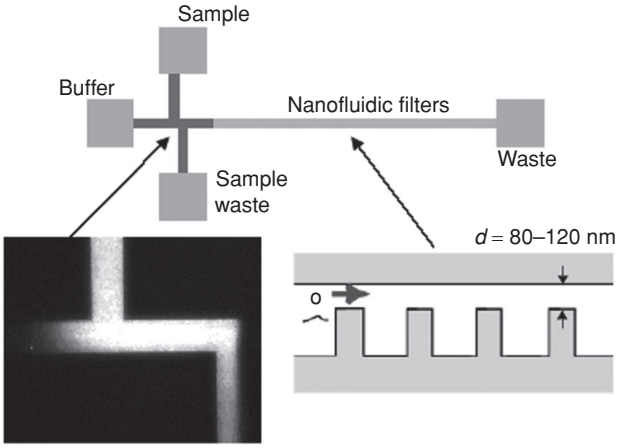

Figure 13.6. Schematic diagram of the nanochannel device for protein separation. (Reprinted with permission from [46] and the IEEE.)

Beside nanochannels, other nanostructures have also been used as "nanosieve" for protein separations, such as "nanofluidic interconnects" in a multilayered microfluidic chip [48] and self-assembly colloidal arrays with ordered nonporous structure embedded inside a microchannel [49].

The two main factors affecting the separation efficiency are solute valence and mobility ratio (virtually the solute diffusivity). Most reports of the protein separation in nanofluidic systems have been achieved by the electric field-driven separation (i.e., electrophoretic separation) that works well for proteins differing in mobility ratio. Alternatively, pressure-driven separation by nanochannels can also be considered to separate proteins with variable valences due to "solute-wall interactions" [50]. The combination of the pressure- and electric field-driven separations in nanochannels has been proposed for more effective separation [50]. In addition, befouling caused by unspecific absorption of the protein onto the surface of the nanofluidic devices should be minimized by approaches such as surface modification with hydrophilic chemical groups or using antibiofouling materials, like PEG, for nanochannel fabrication.

Multidimensional protein separation is an attractive direction to integrate two different separation steps into a single device. It greatly increases the resolution and offers versatility with different separation mechanisms that may be paired in various combinations to enhance selectivity and sensitivity. Currently, multidimensional protein separation has been realized in microfluidic system [51, 52] and there is no multidimensional protein separation system based on nanochannels at present, which may require future efforts.

13.2.2.3 Drug Delivery System Using Nanochannels. Drug delivery devices have been miniaturized from the macroscale (>1 mm) to the microscale

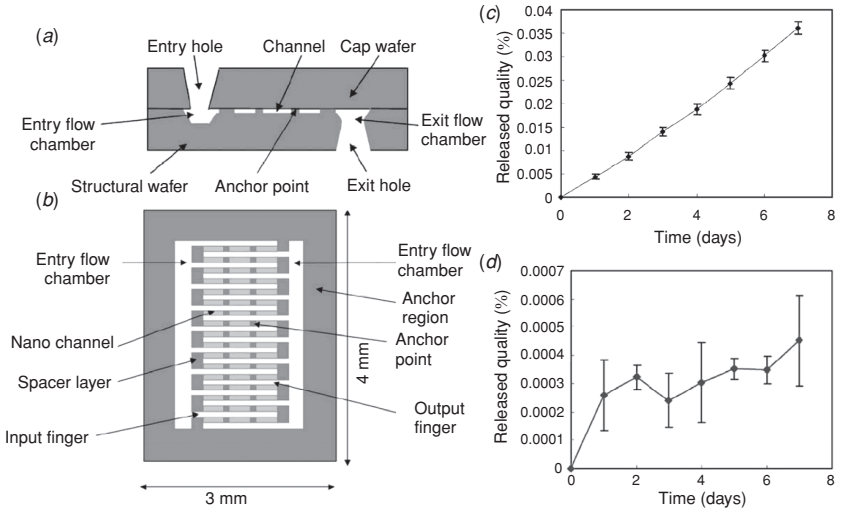

Figure 13.7. (*a*) A cross-sectional view of the nDS. (*b*) A front view of the bottom substrate in the nDS. Release profiles of (*c*) Glucose and (*d*) IFN-α from nDS mounted in Costar diffusion chambers mounted on the wells of a transwell plate. (Reprinted with permission from [55] and the Ovid Technologies, Inc.)

(100–0.1 μm) or nanoscale (100–1 nm) [53]. Nanochannel delivery systems (nDSs) have demonstrated its unique potential to deliver a variety of bioactive molecules at zero-order rates [54]. For example, glucose and IFN-α (an antitumor compound) were delivered directly to the tumor microenvironment at zero-order kinetics by a nDS [55] (Figure 13.7). The compound released from the nanochannels was functionally active on both host immune cells and a human melanoma cell line *in vitro*. The nanochannel drug delivery system could be potentially implanted near the lesion with minimum invasion to provide local, sustained release of antitumor compounds.

In another example, *in vivo* drug delivery has been achieved by using a device containing nanochannels [54]. Top-down nanofabrication techniques were used to create silicon-based nanopores membrane consisting of arrays of uniform nanochannels having a width as small as 7 nm. Using this system, a zero-order release of IFN-α or BSA diffusing through the nanopore was achieved. Following subcutaneous implantation in rats, slow release of protein was demonstrated [56]. This device has good control of channel size and pore distribution, which makes it possible to control the release rate. Q3

The ultimate goal of drug delivery research is to develop implantable drug delivery devices to improve therapeutic efficacy in clinic. Therefore, the future advancement of the nanochannel drug delivery device should have the capacity for drug release patterns other than linear release, which permit studies to determine the optimal release profile for specific therapeutic drugs [55]. Biocompatibility of the device should also be taken into consideration for the successful implantation [57].

Furthermore, future nanochannel drug delivery system should be amenable to external control by a programmable electronic device.

13.3 FABRICATION OF BIOMOLECULAR NANOARRAYS FOR BIOLOGICAL APPLICATIONS

A variety of techniques have been developed to immobilize biomolecules such as DNA, protein, and lipid membrane onto surface with resolutions greater than 1 μm. The selective, precise immobilization of biomolecules with high density possesses high impact in many biological studies. For example, nanoscale arrays of proteins could be used to develop a novel diagnostic method in a rapid and high throughput manner, while patterning peptides could lead to greater control over cell-to-surface interactions. Also, nanoscale arrays can lead to high sensitivity and selectivity of BioNEMS devices with an extremely small amount of reagent. Although, dip-pen lithography [58, 59], photolithography [60], and electron-beam lithography [61–63] have been used to form nanoarray of biomolecules on the surface, these methods have limitations due to complicated fabrication procedures, low speed, or high costs involved.

In this section, we focus on several examples of unconventional patterning methods such as nanoimprinting, nanomolding, and contact printing for the formation of biomolecules nanoarrays. These methods can achieve biomolecular arrays either by directly transferring biomolecules, or by modifying surfaces with a functional chemical or by fabricating templates of adhesion-resistant materials including PEG.

13.3.1 DNA Nanoarray

The controlled placement of DNA molecules onto surfaces is an important process in the fabrication of DNA arrays. A common way to fabricate DNA arrays is to spot fluids containing the desired DNA fragment onto a microscope slide using metal pins [64] or microactuated nozzles [65]. An alternative way was demonstrated by *in situ* synthesis of oligonucleotides (up to 25 bases) using light-activated chemistry combined with photolithographic techniques [66, 67]. A major drawback of these techniques is the inherent sequential, low speed deposition. Therefore, techniques of fabricating arrays on predefined platforms in a parallel fashion would be useful from a production point of view. In this regard, simple printing or molding techniques have been applied to the construction of site-selective template for DNA array [68–72]. For example, Lange et al. used microcontact printing (μCP) with a modified PDMS stamp with positive charges on the surface (Figure 13.8*a*). The stamp was incubated with target DNA molecules in a solution of low pH. The stamp was then rinsed, blown dry, and printed to deliver the DNA to the target surface [69]. Guan et al. fabricated highly ordered arrays of stretched DNA molecules on a large area (up to a millimeter) by using a modified molecular combing method and soft lithography (Figure 13.8*b*) [73]. In this technique, topological micropatterning on PDMS stamps was used to mediate dynamic assembly of DNA molecules into arranged nanostrand

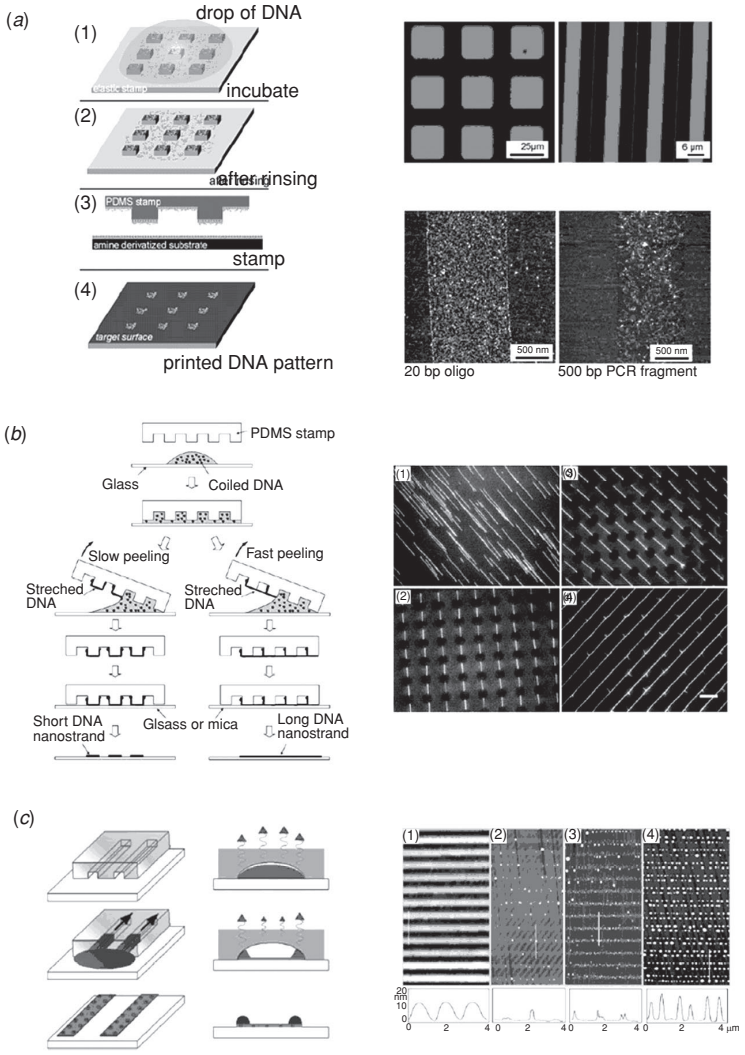

Figure 13.8. Soft-lithographical approach for fabrication of DNA arrays. (*a*) Left: schematic diagram of microcontact printing of DNA molecules; right: fluorescence images of patterned FITC-labeled oligonucleotides on a glass surface after printing and AFM images revealing the printed DNA molecules deposited on mica substrate. AFM images (tapping mode in air) of stamped 1-μm lines of oligonucleotides (left, 20-bp oligos; right, 500-bp PCR fragments) (Reprinted with permission from [69] and the American Chemical Society.) (*b*) Left: schematic of generating and transferring DNA nanostrand arrays; right: fluorescence micrographs of (1) DNA molecules combed on a flat PDMS stamp, (2) vertically and (3) diagonally aligned DNA strands on the PDMS stamps with microwells, and (4) long DNA strands on the PDMS stamp with microwells. (Scale bar, 10 μm.) (Reprinted with permission from [73] and the National Academy of Sciences.) (*c*) Left: deposition of DNA from solution by MIMIC and scale reduction by pinning during the last stages of solvent evaporation; right: AFM images (above) and height profiles (below) of DNA molecules (100–8000 bp) patterned on a mica surface at different concentrations: (1) 1.25 $\mu g\,mL^{-1}$, (2) 2.0 $\mu g\,mL^{-1}$, (3) 2.8 $\mu g\,mL^{-1}$, and (4) 5.0 $\mu g\,mL^{-1}$. (Reprinted with permission from [70] and the Royal Society of Chemistry.)

arrays. The nanostrand arrays were transferred onto flat solid surfaces by contact printing, allowing for the creation of more complex patterns. As shown, stretched DNA molecules on a flat PDMS stamp were generated at a low peeling speed. Depending on the peeling speed, either short or long nanostrands formed. It was also reported that the stretched DNA molecules broke for short nanostrands at the edges of the microwells, resulting in portions in the microwells being untransferred. For long nanostrands, the segments suspended over the microwells were also transferred as those on the top surface of the stamp. Therefore, the authors obtained DNA nanostrands with the monodispersed length determined by the geometry of the micro features on the stamp. Bystrenova et al. [70] fabricated DNA array by MIMIC where dewetting occurred at the last stages of solvent evaporation (Figure 13.8*c*). When the solution was placed at an open end of the cavity, the solution flowed inside driven by capillary forces and surface tension with the boundary walls. Self-organization of the molecular solute occured at the later stages of solvent evaporation. As the solution was pinned to the edges of the channel, the fluid section profile resulted in an inhomogeneous rate of evaporation of the solvent. The convective flow of the solute toward the pinning sites resulted in the precipitation of split structures in the channel. Depending on the concentration, the solute precipitated when the critical concentration was reached. When the concentration of the DNA solution reached 1.25 $\mu g\,mL^{-1}$, the resulting pattern consisted of homogeneous lines. For DNA concentrations between 2 and 4 $\mu g\,mL^{-1}$, the dots were roughly aligned but without well-defined spacing. When the concentration exceeded 5 $\mu g\,mL^{-1}$, spatial correlations emerged among the dots, and the dot size increased. In this case, the dots were perfectly aligned along the edges of the channel as a result of the pinning of the solution and the convective flow from the center toward the edges. The major advantage of soft-lithographical approach is the capability of printing multiple arrays from one loaded stamp. This method could be developed to a potentially cost- and time-saving process, particularly for gene expression studies, where the ratio of bound to labeled molecules matters, but not the total amount of material.

Alternatively, NIL and NIL-related techniques have been used to fabricate arrays of DNA molecules. Ohtake et al. [74, 75] performed DNA nanopatterning on a substrate immobilized with poly-L-lysine by using a nanoimprint process (Figure 13.9). First, poly-L-lysine-coated slide glass was used to immobilize the DNA molecules on a substrate. After imprinting of a poly(vinylalcohol) (PVA) layer and subsequent dry etching, the PVA layer was removed by water. Multiple lines of DNA were patterned and visualized by this approach using a fluorescent-labeled DNA. It was reported that the immobilized DNA pattern was stable due to strong Columbic interactions between positive charges of NH_4^+ in the poly-L-lysine layer and negative charges of PO_4^- in the DNA molecules.

13.3.2 Protein Arrays

The roles of proteins are enormously diverse and include mechanical support, signaling, and sensing. Beyond their central importance to biology, proteins are of great interest because these sub-microscale molecules have the potential to be integrated

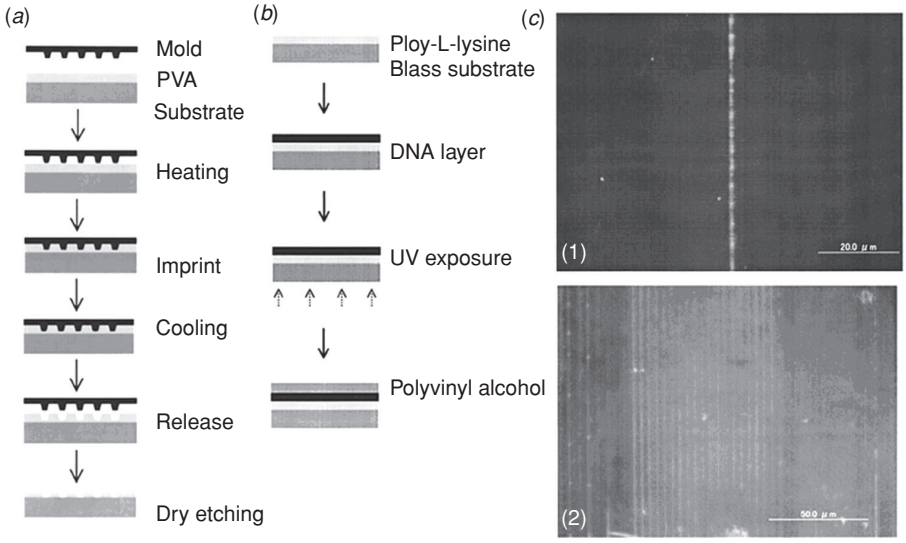

Figure 13.9. NIL and NIL-related techniques for fabrication of DNA arrays. (*a*) Schematic of the nanoimprint process for DNA array. The substrate coated with the PVA was imprinted using a SiO_2/Si mold. (*b*) A preparation process of a DNA substrate by using poly-L-lysine and PVA layers. (*c*) Images of DNA nanopatterns observed with fluorescence microscopy. Single or multiple lines of DNA were seen where the linewidth and spacing were 0.7 and 3 μm, respectively. (Reprinted with permission from [74] and the AVS Science & Technology of Materials, Interfaces, and Processing.)

into BioNEMS devices. For aiming at this application, a nanopatterning technique is necessary, capable of accurately depositing proteins in predefined locations while retaining their native functionality.

Other than spotting [76] or dip-pen nanolithography [59], printing or molding approaches have proven to be successful in fabricating protein arrays. Renault et al. used μCP of single protein molecules on surfaces with the aid of mechanically improved structural features. They have created arrays of posts, ridges, lines, and mesh structures with critical dimensions ranging from 40 to 600 nm (Figure 13.10*a*) [77]. The inking and printing conditions were identical but the patterns printed with a smaller mesh rendered irregular aggregates of proteins that were dispersed on a width of ∼100 nm.

Ross et al. [78] also used μCP with the polymerized lipid bilayers as substrates (Figure 13.10*b*). They demonstrated that printing of BSA onto a dried poly(bisSorbPC) planar supported lipid bilayer (PSLB) from a PDMS stamp produced a layer of strongly adsorbed protein, comparable in surface coverage to films printed on glass surfaces. The dried poly(bisSorbPC) bilayers were contacted with PDMS stamps inked with BSA, rinsed with buffer, and examined for evidence of protein transfer. AFM (atomic force microscope) scans taken over a large area (greater than 100 μm^2) showed that the transferred protein films were very uniform with few defective areas. Q4

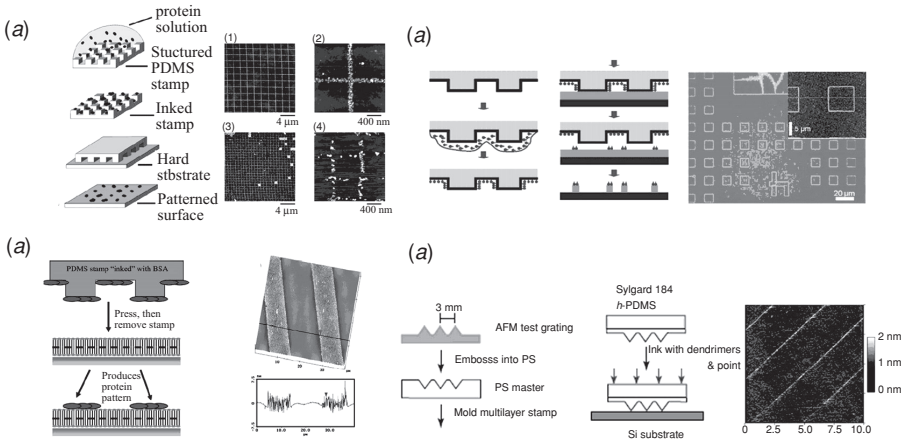

Figure 13.10. Soft-lithographical methods for protein arrays. (*a*) Left: microcontact printing of protein; right: AFM images of antibodies printed on glass using high resolution PDMS stamps. The patterns in (1) and (2) were produced using a grid of 100-nm wide lines that were separated by 2 μm, and the patterns in (3) and (4) used 40-nm wide lines separated by 800 nm. (Reprinted with permission from [77] the American Chemical Society.) (*b*) Left: schematic of contact printing of BSA on a poly(bis-SorbPC) PSLB; right: a representative AFM image and line scan of BSA printed on a poly(bisSorbPC) PSLB from a PDMS stamp. The image size is 40 μm × 40 μm and the height scale is 10 nm. The dark line across the image indicates the position of the line scan. (Reprinted with permission from [78] and the American Chemical Society.) (*c*) Left: schematic of an edge transfer lithography process that employs a surface-modified elastomeric stamp (gray) rendering impermeable and repellent to the applied ink by an applied surface barrier layer (black); right: optical and AFM images and related height profiles (inset) of gold substrates (10-nm-thick gold layer) after printing. (Reprinted with permission from [79] and the American Chemical Society.) (*d*) (left): schematic of nanocontact printing using h-PDMS; (right): AFM image of printed titin multimer protein lines on silicon surface. (Reprinted with permission from [80] and the American Chemical Society.)

Specifically, this procedure could generate an array of fluorescent stripes corresponding to specific binding of avidin to the line pattern of biotinylated BSA.

Sharpe et al. [79] introduced the edge transfer lithography for protein patterning (Figure 13.10*c*). This method is based on the use of the edges of micrometer-sized template features for the reproduction of submicrometer structures. This technique allows for local surface modification in a single step by depositing self-assembled monolayers onto a metal substrate selectively along the feature edges of an elastomeric stamp. Key parameters of a patterning scheme that employs PDMS stamps bearing an isotropic silicon oxide blocking layer are the impermeability of this barrier, and the surface energy compatibility between the stamp surface and the ink. With this approach, large areas could be patterned in a single-step process with dynamic control over feature sizes.

Li et al. introduced the patterning of surfaces via nanocontact printing with chemically distinct features using h-PDMS (hard PDMS) (Figure 13.10*d*) [80]. The extension of contact printing to produce structures in the sub-100-nm scale has been

hampered by two factors. The first factor is the low elastic modulus of Sylgard 184 PDMS stamp, which does not allow the replication of sub-100-nm features. An increase in the Young's modulus of the PDMS improves the mechanical stability of the features on the stamp during printing [81]. The second problem is that the low molecular weight inks (alkanethiols and silanes) lead to diffusion during the printing step, resulting in a limited feature size. The authors used a V-shaped apex whose radius of curvature was approximately 30 nm. With this improved geometry of tip regions, various protein nanoarrays were fabricated by simple contact of inked h-PDMS mold.

Alternatively, NIL was used for protein patterning of high density with feature size below 100 nm, while retaining high throughput and reproducibility (Figure 13.11*a*) [82, 83]. In one example, a (CF*x*)*n* polymer ($x = 1$ or 2, $n =$ number of

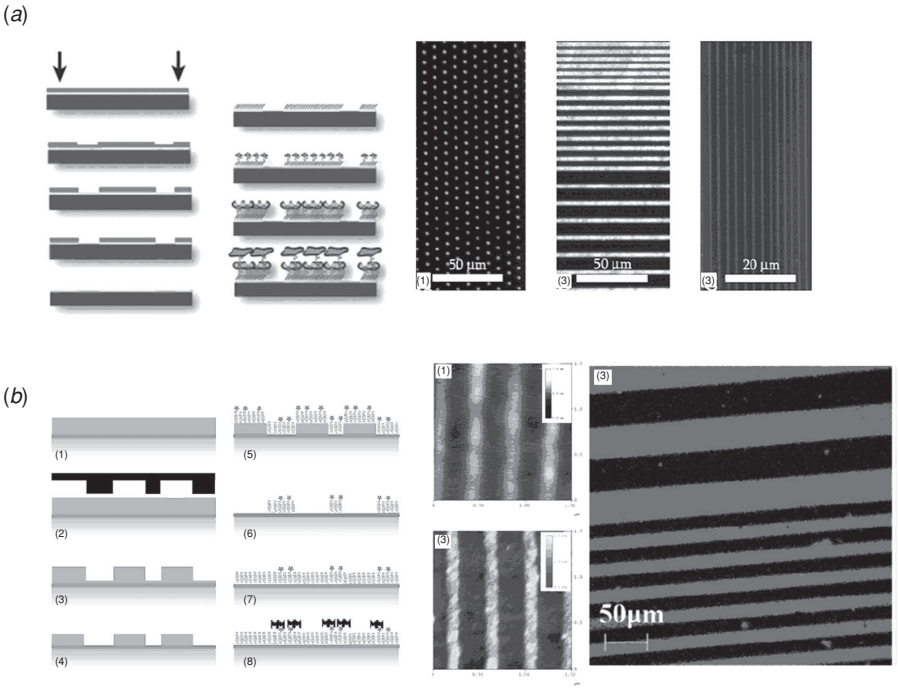

Figure 13.11. Examples of the nanoimprint process for fabrication of protein array. (*a*) Left: process flow diagram of substrate patterning and protein immobilization; right: epi-fluorescence image of rhodamine-labeled streptavidin bound to sharp uniform microscale dots (1) and lines (2) of biotinylated BSA protein on oxidized Si substrates. (3) Rhodamine-labeled streptavidin bound to patterns of immobilized biotinylated BSA on cover glass. (Reprinted with permission from [83] and the American Chemical Society.) (*b*) Left: schematic of combining NIL and molecular assembly patterning; (1) AFM scans of PLL-*g*-PEG/PEG-biotin stripes in an oxide background and (2) After PLL-*g*-PEG backfill the pattern is still visible due to the longer PEG chains supporting the biotin molecules (3) confocal laser scanning microscope (CLSM) image. (Reprinted with permission from [82] and the American Chemical Society.)

monomer subunits, monomer $M_W = 31$ or 50) was deposited during a CHF3 RIE procedure for shielding adsorption of protein. The exposed oxide pattern selectively reacts with an aminosilane to form a covalently bound monolayer. The target protein was bound by flushing the flowcell with a 50 μg/mL biotinylated BSA solution in blocking buffer and incubating for 10 min. This technique achieved high throughput, reproducible nanoscale protein patterns with high selectivity and functionality, as measured by covalent bonding between patterned antibodies and their antigen.

Falconnet et al. [82] developed a protein patterning method by combining NIL and molecular assembly patterning by liftoff (Figure 13.11*b*). A heated PMMA film was imprinted by a mold, followed by a dry etching step that converted the topography into a PMMA/Nb2O5 contrast. A biotin functionalized copolymer, poly(L-lysine)-*graft*-poly(ethylene glycol)-biotin (PLL-*g*-PEG/PEG-biotin), spontaneously adsorbed on the oxide surfaces. To inhibit nonspecific protein adsorption in the background, the Nb2O5 areas were rendered nonfouling by spontaneous adsorption of the nonfunctionalized PLL-*g*-PEG from an aqueous solution. After PMMA liftoff, the background was backfilled with protein-resistant PLL-*g*-PEG. They demonstrated that the streptavidin lines displayed an excellent contrast between the biotinylated areas and the PLL-*g*-PEG background. No fluorescent signal could be detected on the PEG background.

Zhu et al. [84] described a rapid chemomechanical technique to fabricate width-adjustable extracellular matrices (ECM) protein for the study of cell adhesion (Figure 13.12*a*). The fabrication technique created nano- to microscale patterns starting from no pattern at all using simple procedures and equipment. The widths of the cracks (120–3200 nm) were similar in size to individual adhesion complexes (typically 500–3000 nm^2) and can be modulated by adjusting the mechanical strain applied to the substrate. The cracks expose underlying material—the sidewalls of the cracks—onto which proteins were adsorbed. When the adsorbed proteins are cell adhesive and cell accessible, the patterned substrate supports cell attachment and spreading. Using this approach, they patterned a variety of proteins and demonstrated patterned attachment, spreading, and retraction of various types of cells along ECM protein-adsorbed cracks.

Suh et al. demonstrated fabrication of protein patterns by using CFL technique with a nonbiofouling polymer material as the template layer against protein adsorption, resulting in patterned cell arrays [86–89]. They used nanowell patterns of a PEG-based random copolymer, poly(3-trimethoxysilyl)propyl methacrylate-*r*-poly(ethylene glycol) methyl ether) [poly(TMSMA-*r*-PEGMA)] with good physical integrity (Figure 13.12*b*) [85]. The height of patterns ranged from a few nanometers to a few hundred nanometers, serving as a migration barrier to maintain a sharp boundary between patterned and nonpatterned regions. This PEG copolymer has an anchoring group and thus can bind covalently to silicon surfaces, allowing for excellent water stability for at least 2 weeks. Using PDMS molds, 700-nm nanowells were fabricated on silicon wafer over a large area with a barrier height of ∼280 nm. The incubation of an antibody onto the PEG template resulted in a selective adsorption of the antibody onto the exposed substrate because the PEG copolymer surface is highly resistant to protein adhesion.

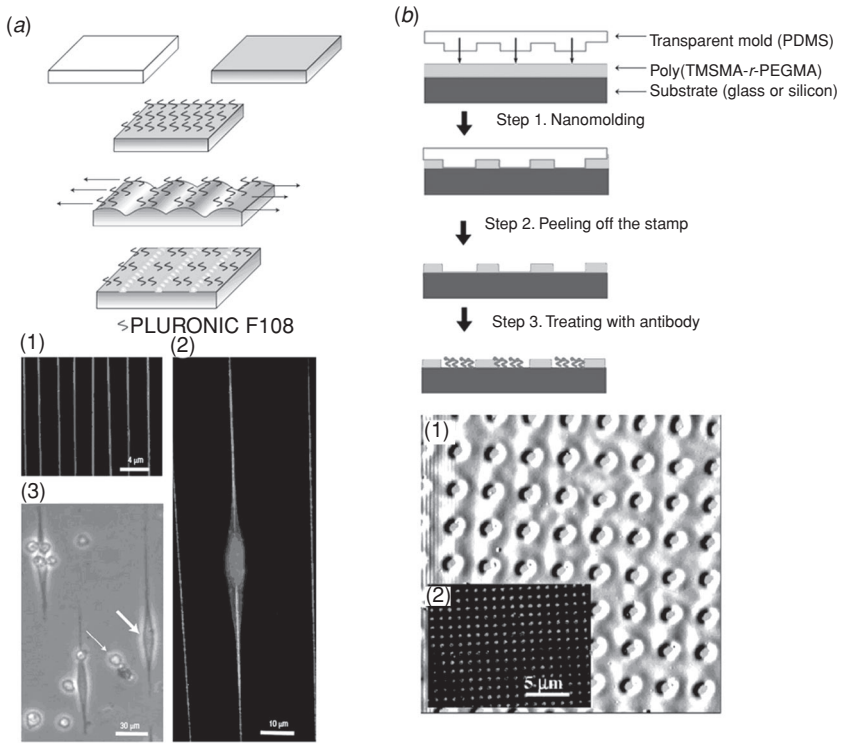

Figure 13.12. (*a*) Schematic illustration of crack patterning; (1): parallel cracks formed by the procedure using fluorescent protein (FITC-BSA); (2): a micrograph of C2C12 myoblasts spread on wide cracks; and (3) a C2C12 myoblast cell stained with phalloidin-TRITC for actin (red), Hoechst 33342 for the nucleus (blue). The cell is attached to a crack coated with collagen (green). (Reprinted with permission from [84] and the Nature Publishing Group.) (*b*) Schematic illustration of nanomolding for protein patterning; (1) AFM images of 700-nm PEG nanowells in deflection mode; (2) the corresponding fluorescent image treated with the P3 antibody and a FITC-labeled secondary antibody image. (Reprinted with permission from [85] and the American Chemical Society.)

13.3.3 Lipid Array

Cellular membranes contain many proteins that regulate molecular interactions. Of these, receptor proteins play a central role in cell signaling. Because lipid bilayers are held together by hydrophilic and hydrophobic interactions, biomolecules embedded in these structures are free to diffuse laterally. Q11

Preparation of arrays of lipid bilayer or membrane is important since the binding event is highly specific and varies depending on the targeting strategy employed (e.g., chemical linking, physical binding, or biospecific recognition). Lipid membranes are a highly efficient biosensing platform for electrochemical detection of ligand–receptor interactions, cellular attack, or signal transduction [90–92]. Furthermore, the inclusion of multiple functional groups on the surface is beneficial in the 2D geometry of the lipid membranes [93].

In 1997, Groves et al. [94] first introduced a microfabrication method for patterning surfaces with solid supported phospholipid bilayers. The method involved the patterning of photoresist on fused quartz wafers by means of standard photolithographic techniques. Since then, a number of methods have been developed for microarrays of lipid membrane, such as deep-UV illumination through a photomask under aqueous conditions [95, 96] and polymer liftoff method [97–100]. μCP of composition arrays of phospholipids bilayers was first accomplished by printing different-sized bilayers of the same composition into surface patterned corrals [101–103]. Also, MIMIC technique was used to pattern lipid membranes by utilizing a laminarly flowing stream [104–106]. The use of laminar flow inside microfluidic channels is also an effective means of producing composition arrays of supported phospholipid bilayers in which two distinct chemical components can be varied simultaneously along a one-dimensional gradient [104, 107].

Recently, CFL was used to create patterns of supported lipid bilayer (SLB) membranes onto a surface (Figure 13.13). Micro- or nanopatterns of a PEG random copolymer were fabricated on glass substrates by CFL to form a template layer against adsorption of lipid membranes [108]. As compared to μCP, the molded structures provided a clean interface at the patterned boundary and the adhesion on the PEG surface was strongly restricted. The functionality of the patterned SLBs was tested by measuring the binding interactions between biotin-labeled lipid bilayer and streptavidin. SLB arrays were fabricated with spatial resolution down to ∼500 nm on flat substrate and ∼1 μm inside microfluidic channels, respectively.

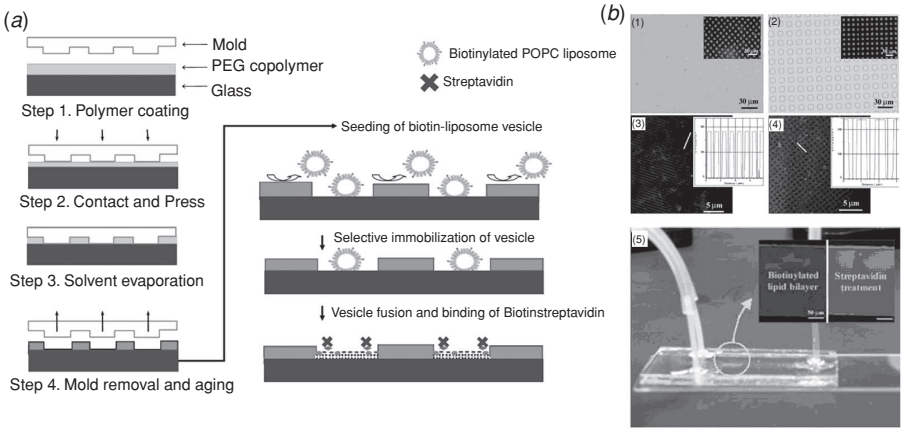

Figure 13.13. (*a*) A schematic diagram for patterning supported bilayer membranes (SBMs) by using CFL of a PEG-based copolymer. (*b*) Resulting micro- and nanopatterns of SBMs. (1), (2) Optical images of the PEG patterns and fluorescent images of the biotinylated lipid layers (inset) using microcontact printing (1) and CFL (2). The 10 μm box pattern was used for both methods. (3), (4) Fluorescent micrographs of the sub-micrometer patterns of biotinylated SBMs along with intensity profiles using CFL: (3) 500 nm lanes and (4) 500 nm grids. (5) A simple Y-shaped channel combined with nanoarrays of biotin (red) and streptavidin (green) after binding reaction. (Reprinted with permission from [108] and the Royal Society of Chemistry.)

Au: R.H. ok?

13.4 FABRICATION OF NANOSCALE TOPOGRAPHIES FOR TISSUE ENGINEERING APPLICATIONS

Living tissues are ensembles of different cell types embedded in complex and well-defined structures of ECM with nanoscale topographical features. Frequently, the organization of ECM is hierarchical in that large-scale protein structures up to several hundred micrometers are found, which are covered with intricate nanoscale features. For example, hierarchical assembly of collagen molecules can lead to formation of fibrils, long (tens of microns) cylindrical structures, whose diameter may vary in 20–200 nm range. In connective tissues, it is also common to find bundles of collagen microfibrils running in parallel to each other, with cells of various origins attached to them. These cells might both affect and be affected by the super-structures of collagen and other ECM components.

Thus, it could greatly improve our understanding on how cell–ECM interactions affect cellular processes if one could build up ECM nanopatterns on various 2D and three-dimensional (3D) substrates. A few nanopatterning approaches have been proposed to produce ECM protein patterns at the nanoscale and to control the spatial distribution of ECM proteins. For example, scanning probe lithography (SPL)-based methods were used to print collagens and collagen-like peptides (30–50 nm linewidth) without disrupting the triple-helical structures and biological activities of collagens [109, 110]. Nanopatterning of self-assembled monolayers by EBL has been developed to produce organic templates for creating high density protein nanoarrays [111, 112]. Selective molecular assembly patterning in combination with lithographically prepatterned substrate also has been proven as a fast and reliable method to create protein arrays over large areas with feature sizes comparable to SPL-based techniques [113–118].

Here, we focus on simple printing or molding techniques for incorporating complex nanostructures into an underlying substratum to mimic various *in vivo* 3D ECM environments with structural and mechanical similarity. These methods are of high significance due to its potential to yield both fundamental knowledge of mechanisms governing cell motility and the resulting control of cellular function that can be used in advanced tissue engineering.

13.4.1 Nanotopography-Induced Changes in Cell Adhesion

Recently, CFL has been used to create various nanotopographies of UV-curable PEG hydrogel on glass substrate by using a new UV-curable mold made from acrylate groups poly(urethaneacrylate) (PUA)-functionalized polyurethane (Figure 13.14) [114]. It was found that proteins (collagen, fibronectin, immunoglobulin, and albumin) and cells (CHO, fibroblasts, and P19 EC cells) preferred to adhere on nanostructured PEG surfaces in comparison to unpatterned PEG films. However, the level of adhesion was significantly lower than that of glass controls. These results agree with other studies such that surface nanotopography enhances the cell-substratum adhesion of human corneal epithelial cells [119] and primary rat cardiomyocytes [120]. Other studies using CFL revealed that the wetting property of the nanostructured

Q5

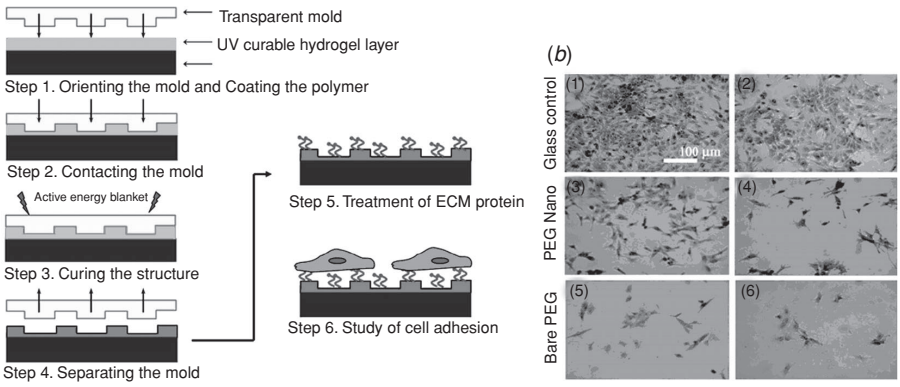

Figure 13.14. (*a*) A schematic procedure of UV-assisted nanomolding of PEG hydrogel using CFL technique. (*b*) Optical micrographs of the stained P19 EC cells adhered on glass, bare PEG, and a PEC nanostructured surface in the presence of collagen (1), (3), (5) and in the absence of collagen (2), (4), (6). The cells were cultured for 2 days.

surface of a given chemical composition can be systematically controlled by rendering nanoscale roughness [121]. These findings suggest that the control over wettability by surface nanotopography can also modulate spatial distribution of absorbed proteins and cell adhesion properties. However, the role played by the adhesive ECM proteins coated on the nanostructured polymeric surface on cell adhesion has not been extensively addressed. Further studies by combining nanoscale mechanical topography and adhesive ECM nanopatterns on polymer cell culture substrates possibly provide more insights on how cells interact with surface nanotopography and surface adhesive nanopattern, respectively [122].

13.4.2 Nanotopography-Induced Changes in Cell Morphology

It has been found that nanotopography induces change in morphology and motility of many different cell types, which is also called "contact guidance." Contact guidance refers to the reactions of cells with the topography of their substratum [123, 124]. Arrays of parallel nanogrooves (alternatively nanoridges) have been fabricated by nanoimprint or UV photolithography to provide an *in vitro* experimental model for investigating how nanotopography of the *in vivo* ECM can affect cell motility. Further quantitative analysis with corneal epithelial cells showed that the percentage of aligned cells was constant on the substrate topographies with lateral dimensions ranging from 70 nm to 2 μm, and increased with groove depth ranging from 150 to 600 nm [125]. Interestingly, recent ultrastructural analysis showed that primary human corneal epithelial cells oriented perpendicular to 400-nm pitch patterns (70 nm ridges) extended filopodia in a crown-like fashion with individual filopodium having orientations that were perpendicular, oblique or parallel to the underlying pattern (Figure 13.15) [126]. In contrast, in cells that were aligned parallel to larger scale

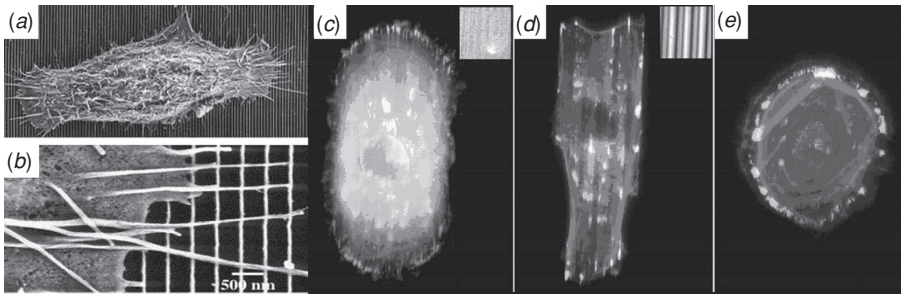

Figure 13.15. Nanotopography-induced change in morphology and motility. (*a*), (*b*) SEM images of perpendicularly aligned cell on 70-nm wide ridges on a 400 nm pitch. (Reprinted with permission from [126] and the Elsevier B.V.). Immunofluorescent micrographs of cells on (*c*) a substrate with 600-nm deep grooves and 70-nm wide ridges on a 400 nm pitch, (*d*) a substrate with 600-nm deep grooves and 1900 nm ridges on a 4000 nm pitch, and (*e*) a smooth silicon oxide substrate, respectively, stained for actin (red), vinculin (green), and the nucleus (blue). Insets: a reflection image of the substrates. (Reprinted with permission from [125] and the Company of Biologists Ltd.)

patterns (4000 nm pitch, 1900 nm ridges), filopodia were generally more guided by the substrate topographies resulting in most filopodia extending parallel to the underlying features [126].

Details on cell–substrate interactions in cell biology and tissue engineering applications can be found in an extensive review paper and reference therein [4]. It is envisioned that better understanding of signaling and cellular functions through the nanoscale control of cell-ECM interaction could open up novel strategies to achieve targeted cell functions in tissue engineering applications.

REFERENCES

1. Mrksich, M., Chen, C. S., Xia, Y. N., Dike, L. E., Ingber, D. E., and Whitesides, G. M. (1996) Controlling cell attachment on contoured surfaces with self-assembled monolayers of alkanethiolates on gold. *Proc. Natl. Acad. Sci. USA* **93**, 10775–10778.
2. Whitesides, G. M., Ostuni, E., Takayama, S., Jiang, X. Y., and Ingber, D. E. (2001) Soft lithography in biology and biochemistry. *Annu. Rev. Biomed. Eng.* **3**, 335–373.
3. Yim, E. K. F., Reano, R. M., Pang, S. W., Yee, A. F., Chen, C. S., and Leong, K. W. (2005) Nanopattern-induced changes in morphology and motility of smooth muscle cells. *Biomaterials* **26**, 5405–5413.
4. Sniadecki, N., Desai, R. A., Ruiz, S. A., and Chen, C. S. (2006) Nanotechnology for cell-substrate interactions. *Ann. Biomed. Eng.* **34**, 59–74.
5. Shin, H. (2007) Fabrication methods of an engineered microenvironment for analysis of cell-biomaterial interactions. *Biomaterials* **28**, 126–133.
6. Wikswo, J. P., Prokop, A., Baudenbacher, F., Cliffel, D., Csukas, B., and Velkovsky, M. (2006) Engineering challenges of BioNEMS: the integration of microfluidics, micro- and

nanodevices, models and external control for systems biology. *IEE Proc., Nanobiotechnol*. **153**, 81–101.

7. Pearson, D. R. S. C. J. L. (2005) A single-step process for making nanofluidic channels using electron beam lithography. *Microelectron. Eng*. **78–79**, 343–348.
8. Liao, K., Yao, N., and Kuo, T. (2006) Sub-60 nm nanofluidic channels fabricated by glass-glass bonding. *Proceedings of the 28th IEEE*, pp. 2832–2835.
9. Kovarik, M. L. and Jacobson, S. C. (2007) Attoliter-scale dispensing in nanofluidic channels. *Anal. Chem*. **79**, 1655–1660.
10. Karnik, R., Castelino, K., Fan, R., Yang, P., and Majumdar, A. (2005) Effects of biological reactions and modifications on conductance of nanofluidic channels. *Nano Lett*. **5**, 1638–1642.
11. Turner, S. W., Cabodi, M., and Craighead, H. G. (2002) Confinement-induced entropic recoil of single DNA molecules in a nanofluidic structure. *Phys. Rev. Lett*. **88**, 128103.
12. Reccius, C. H., Mannion, J. T., Cross, J. D., and Craighead, H. G. (2005) Compression and free expansion of single DNA molecules in nanochannels. *Phys. Rev. Lett*. **95**, 268101.
13. Mijatovic, D., Eijkel, J. C., and Van Den Berg, A. (2005) Technologies for nanofluidic systems: top-down vs. bottom-up—a review. *Lab Chip* **5**, 492–500.
14. Mao, P. and Han, J. (2005) Fabrication and characterization of 20 nm planar nanofluidic channels by glass-glass and glass-silicon bonding. *Lab Chip* **5**, 837–844.
15. Chapman, H. N., Ray-Chaudhuri, A.K., Tichenor, D.A., Replogle, W.C., Stulen, R.H., Kubiak, G.D., Rockett, P.D., Klebanoff, L.E., et. al. (2001) First lithographic results from the extreme ultraviolet engineering test stand. *J. Vac. Sci. Technol. B* **19**, 2389–2395.
16. Naulleau, P. (2002) Sub-70 nm extreme ultraviolet lithography at the advanced light source static microfield exposure station using the engineering test stand set-2 optic. *J. Vac. Sci. Technol. B* **20**, 2829–2833.
17. Danelon, C., Santschi, C., Brugger, J., and Vogel, H. (2006) Fabrication and functionalization of nanochannels by electron-beam-induced silicon oxide deposition. *Langmuir* **22**, 10711–10715.
18. Wang, K., Yue, S., Wang, L., Jin, A., Gu, C., Wang, P., Wang, H., Xu, X., et al. (2006) Nanofluidic channels fabrication and manipulation of DNA molecules. *IEE Proc. Nanobiotechnol*. **153**, 11–15.
19. Kaige, W., Pengye, W., Hong, W., Changzhi, G., Shuanglin, Y., Aizi, J., Wenqing, L., and Hanben, N. (2005) Fabricating nanofluidic channels and applying it for single biomolecule study. *Conf. Proc. IEEE Eng. Med. Biol. Soc*. **2**, 1278–1281.
20. OBrien, M. J., II, Bisong, P., Ista, L. K., Rabinovich, E. M., Garcia, A. L., Sibett, S. S., Lopez, G. P., and Brueck, R. (2003) Fabrication of an integrated nanofluidic chip using interferometric lithography. *J. Vac. Sci. Technol. B* **21**, 2941.
21. Müllenborn, M., Dirac, H., and Petersen, J. W. (1995) Three-dimensional nanostructures by direct laser etching of Si. *Appl. Surf. Sci*. **86,** 568–576.
22. Hui, A. P., Shui-jie, Q., Li, W. J., and Wang, M. Y. (2002) High aspect ratio nano fluidic channels by laser controlled fracturing. *The 15th IEEE International Conference on Micro Electro Mechanical Systems*, pp. 156–159.
23. Anpan, H., Nicolaas, F. D. R., and Urs, S. (2006) Design and fabrication of nanofluidic devices by surface micromachining. *Nanotechnology* **86,** 2498–2503.

24. Truskett, V. N. and Watts, M. P. (2006) Trends in imprint lithography for biological applications. *Trends Biotechnol*. **24**, 312–317.
25. Abgrall, P., Low, L. N., and Nguyen, N. T. (2007) Fabrication of planar nanofluidic channels in a thermoplastic by hot-embossing and thermal bonding. *Lab Chip* **7**, 520–522.
26. Cao, H., Yu, Z., Wang, J., and Zhou, S. Y. (2002) Fabrication of 10 nm enclosed nanofluidic channels. *Appl. Phys. Lett*. **81**, 174–176.
27. Tegenfeldt, J. O., Prinz, C., Cao, H., Chou, S., Reisner, W. W., Riehn, R., Wang, Y. M., Cox, E. C., et al. (2004) From the cover: the dynamics of genomic-length DNA molecules in 100-nm channels. *Proc. Natl. Acad. Sci. USA* **101**, 10979–10983.
28. Wang, X., Chen, Y., Banu, S., Morgan, H., Fu, S., and Cui, Z. (2007) High density patterns fabricated in SU-8 by UV curing nanoimprint. *Microelectron. Eng*. **84**, 872–876.
29. Kim, P., Jeong, H. E., Khademhosseini, A. and Suh, K. Y. (2006) Fabrication of nonbiofouling polyethylene glycol micro- and nanochannels by ultraviolet-assisted irreversible sealing. *Lab Chip* **6**, 1432–1437.
30. Lensen, M. C., Mela, P., Mourran, A., Groll, J., Heuts, J., Rong, H., and Moller, M. (2007) Micro- and nanopatterned star poly(ethylene glycol) (PEG) materials prepared by UV-based imprint lithography. *Langmuir* **23**, 7841–7846.
31. Lee, N. Y., Lim, J. R., Lee, M. J., Kim, J. B., Jo, S. J., Baik, H. K., and Kim, Y. S. (2006) Hydrophilic composite elastomeric mold for high-resolution soft lithography. *Langmuir* **22**, 9018–9022.
32. Ilic, B., Czaplewski, D., Zalalutdinov, M., Schmidt, B., and Craighead, H. G. (2002) Fabrication of flexible polymer tubes for micro and nanofluidic applications. *J. Vac. Sci. Technol. B* **20**, 2459–2465.
33. Kim P. and Suh, K. Y. (2007) Rigiflex, spontaneously wettable polymeric mold for forming reversibly bonded nanocapillaries. *Langmuir* **23**, 4549–4553.
34. Huh, D., Mills, K. L., Zhu, X., Burns, M. A., Thouless, M. D., and Takayama, S. (2007) Tuneable elastomeric nanochannels for nanofluidic manipulation. *Nat. Mater.* **6**, 424–428.
35. Park, K. S., Seo, E. K., Do, Y. R., Kim, K., and Sung, M. M. (2006) Light stamping lithography: microcontact printing without Inks. *J. Am. Chem. Soc*. **128**, 858–865.
36. Slater, G. W., Desruisseaux, C., Hubert, S. J., Mercier, J. F., Labrie, J., Boileau, J., Tessier, F., and Pepin, M. P. (2000) Theory of DNA electrophoresis: a look at some current challenges. *Electrophoresis* **21**, 3873–3887.
37. Lin, J., Qi, R., Aston, C., Jing, J., Anantharaman, T. S., Mishra, B., White, O., Daly, M. J., et al. (1999) Whole-genome shotgun optical mapping of deinococcus radiodurans. *Science* **285**, 1558–1562.
38. Riehn, R., Lu, M., Wang, Y. M., Lim, S. F., Cox, E. C., and Austin, R. H. (2005) Restriction mapping in nanofluidic devices. *Proc. Natl. Acad. Sci. USA* **102**, 10012–10016.
39. Dukkipati, V. R., Kim, J. H., Pang, S. W., and Larson, R. G. (2006) Protein-assisted stretching and immobilization of DNA molecules in a microchannel. *Nano Lett*. **6**, 2499–2504.
40. Herrick, J. and Bensimon, A. (1999) Single molecule analysis of DNA replication. *Biochimie* **81**, 859–871.

41. Strick, T., Allemand, J., Croquette, V., and Bensimon, D. (2000) Twisting and stretching single DNA molecules. *Prog. Biophys. Mol. Biol.* **74**, 115–140.
42. Mannion, J. T., Reccius, C. H., Cross, J. D., and Craighead, H. G. (2006) Conformational analysis of single DNA molecules undergoing entropically induced motion in nanochannels. *Biophys. J.* **90**, 4538–4545.
43. Cao, H., Tegenfeldt, J. O., Austin, R. H., and Chou, S. Y. (2002) Gradient nanostructures for interfacing microfluidics and nanofluidics. *Appl. Phys. Lett.* **81**, 3058–3060.
44. Bakajin, O. B., Duke, T. A. J., Chou, C. F., Chan, S. S., Austin, R. H., and Cox, E. C. (1998) Electrohydrodynamic stretching of DNA in confined environments. *Phys. Rev. Lett.* **80**, 2737.
45. Stein, D., Van Der Heyden, F. H., Koopmans, W. J., and Dekker, C. (2006) Pressure-driven transport of confined DNA polymers in fluidic channels. *Proc. Natl. Acad. Sci. USA* **103**, 15853–15858.
46. Han, J. and Fu, J. (2004) Biomolecule separation by steric hindrance using nanofluidic filters. *Conf. Proc. IEEE Eng. Med. Biol. Soc.* **4**, 2611–2614.
47. Wang, Y. C., Stevens, A. L., and Han, J. (2005) Million-fold preconcentration of proteins and peptides by nanofluidic filter. *Anal. Chem.* **77**, 4293–4299.
48. Flachsbart, B. R., Wong, K., Iannacone, J. M., Abante, E. N., Vlach, R. L., Rauchfuss, P. A., Bohn, P. W., Sweedler, J. V., et al. (2006) Design and fabrication of a multilayered polymer microfluidic chip with nanofluidic interconnects via adhesive contact printing. *Lab Chip* **6**, 667–674.
49. Zeng, Y. and Harrison, D. J. (2007) Self-assembled colloidal arrays as three-dimensional nanofluidic sieves for separation of biomolecules on microchips. *Anal. Chem.* **79**, 2289–2295.
50. Xuan, X. and Li, D. (2007) Solute separation in nanofluidic channels: pressure-driven or electric field-driven?. *Electrophoresis* **28**, 627–634.
51. Wang, Y. C., Choi, M. H., and Han, J. (2004) Two-dimensional protein separation with advanced sample and buffer isolation using microfluidic valves. *Anal. Chem.* **76**, 4426–4431.
52. Li, Y., Buch, J. S., Rosenberger, F., DeVoe, D. L., and Lee, C. S. (2004) Integration of isoelectric focusing with parallel sodium dodecyl sulfate gel electrophoresis for multidimensional protein separations in a plastic microfluidic [Correction of microfludic] network. *Anal. Chem.* **76**, 742–748.
53. LaVan, D. A., McGuire, T., and Langer, R. (2003) Small-scale systems for in vivo drug delivery. *Nat. Biotechnol.* **21**, 1184–1191.
54. Martin, F., Walczak, R., Boiarski, A., Cohen, M., West, T., Cosentino, C., Shapiro, J., and Ferrari, M. (2005) Tailoring width of microfabricated nanochannels to solute size can be used to control diffusion kinetics. *J. Control Release* **102**, 123–133.
55. Lesinski, G. B., Sharma, S., Varker, K. A., Sinha, P., Ferrari, M., and Carson, W. E. (2005) Release of biologically functional interferon-alpha from a nanochannel delivery system. *Biomed. Microdevices* **7**, 71–79.
56. Staples, M., Daniel, K., Cima, M. J., and Langer, R. (2006) Application of micro- and nano-electromechanical devices to drug delivery. *Pharm. Res.* **23**, 847–863.
57. Voskerician, G., Shive, M. S., Shawgo, R. S., von Recum, H., Anderson, J. M., Cima, M. J., and Langer, R. (2003) Biocompatibility and biofouling of MEMS drug delivery devices. *Biomaterials* **24**, 1959–1967.

58. Piner, R. D., Zhu, J., Xu, F., Hong, S. H., and Mirkin, C. A. (1999) "Dip-Pen" nanolithography. *Science* **283**, 661–663.

59. Lee, K. B., Park, S. J., Mirkin, C. A., Smith, J. C., and Mrksich, M. (2002) Protein nanoarrays generated by dip-pen nanolithography. *Science* **295**, 1702–1705.

60. Schena, M., Shalon, D., Heller, R., Chai, A., Brown, P. O., and Davis, R. W. (1996) Parallel human genome analysis: microarray-based expression monitoring of 1000 genes. *Proc. Natl. Acad. Sci. USA* **93**, 10614–10619.

61. Pallandre, A., Glinel, K., Jonas, A. M., and Nysten, B. (2004) Binary nanopatterned surfaces prepared from silane monolayers. *Nano Lett.* **4**, 365–371.

62. Harnett, C. K., Satyalakshmi, K. M., and Craighead, H. G. (2001) Bioactive templates fabricated by low-energy electron beam lithography of self-assembled monolayers. *Langmuir* **17**, 178–182.

63. Borini, S., D'Auria, S., Rossi, M., and Rossi, A. M. (2005) Writing 3D protein nanopatterns onto a silicon nanosponge. *Lab Chip* **5**, 1048-1052.

64. Shalon, D., Smith, S. J., and Brown, P. O. (1996) A DNA microarray system for analyzing complex DNA samples using two-color fluorescent probe hybridization. *Genome Res.* **6**, 639–645.

65. Schober, A., Gunther, R., Schwienhorst, A., Doring, M., and Lindemann, B. F. (1993) Accurate high-speed liquid handling of very small biological samples. *Biotechniques* **15**, 324–329.

66. Lipshutz, R. J., Fodor, S. P. A., Gingeras, T. R., and Lockhart, D. J. (1999) High density synthetic oligonucleotide arrays. *Nat. Genet.* **21**, 20–24.

67. Fodor, S. P. A., Read, J. L., Pirrung, M. C., Stryer, L., Lu, A. T., and Solas, D. (1991) Light-directed, spatially addressable parallel chemical synthesis. *Science* **251**, 767–773.

68. Matsumoto, F., Kamiyama, M., Nishio, K., and Masuda, H. (2005) Highly ordered nanopatterning of DNA with 40 nm diameter using anodic porous alumina substrate. *Japan. J. Appl. Phys. Part 2: Lett. Express Lett.* **44**, L355–L358.

69. Lange, S. A., Benes, V., Kern, D. P., Horber, J. K. H., and Bernard, A. (2004) Microcontact printing of DNA molecules. *Anal. Chem.* **76**, 1641–1647.

70. Bystrenova, E., Facchini, M., Cavallini, M., Cacace, M. G., and Biscarini, F. (2006) Multiple length-scale patterning of DNA by stamp-assisted deposition. *Angew. Chem.Int. Ed.* **45**, 4779–4782.

71. Zhang, G. J., Tanii, T., Funatsu, T., and Ohdomari, I. (2004) Patterning of DNA nanostructures on silicon surface by electron beam lithography of self-assembled monolayer. *Chem. Commun.* 786–787.

72. Shin, J. S. (2004) Rewritable memory by controllable nanopatterning of DNA. *Abstr. Papers Am. Chem. Soc.* **227**, U241–U241.

73. Guan, J. J. and Lee, J. (2005) Generating highly ordered DNA nanostrand arrays. *Proc. Natl. Acad. Sci. USA* **102**, 18321–18325.

74. Ohtake, T., Nakamatsu, K., Matsui, S., Tabata, H., and Kawai, T. (2004) DNA nanopatterning with self-organization by using nanoimprint. *J. Vac. Sci. Technol. B* **22**, 3275–3278.

75. Ohtake, T., Nakamatsu, K., Matsui, S., Tabata, H., and Kawai, T. (2006) Novel DNA nano-patterning design method utilizing poly-L-lysine patterning by nanoimprint lithography. *J. Nanosci. Nanotechnol.* **6**, 2187–2190.

76. Bergman, A. A., Buijs, J., Herbig, J., Mathes, D. T., Demarest, J. J., Wilson, C. D., Reimann, C. T., Baragiola, R. A., et al. (1998) Nanometer-scale arrangement of human serum albumin by adsorption on defect arrays created with a finely focused ion beam. *Langmuir* **14**, 6785–6788.
77. Renaultt, J. P., Bernard, A., Bietsch, A., Michel, B., Bosshard, H. R., Delamarche, E., Kreiter, M., Hecht, B., et al. (2003) Fabricating arrays of single protein molecules on glass using microcontact printing. *J. Phys. Chem. B* **107**, 703–711.
78. Ross, E. E., Joubert, J. R., Wysocki, R. J., Nebesny, K., Spratt, T., O'Brien, D. F., and Saavedra, S. S. (2006) Patterned protein films on poly(lipid) bilayers by microcontact printing. *Biomacromolecules* **7**, 1393–1398.
79. Sharpe, R. B. A., Titulaer, B. J. F., Peeters, E., Burdinski, D., Huskens, J., Zandvliet, H. J. W., Reinhoudt, D. N., and Poelsema, B. (2006) Edge transfer lithography using alkanethiol inks. *Nano Lett*. **6**, 1235–1239.
80. Li, H. W., Muir, B. V. O., Fichet, G., and Huck, W. T. S. (2003) Nanocontact printing: a route to sub-50-nm-scale chemical and biological patterning. *Langmuir* **19**, 1963–1965.
81. Schmid, H. and Michel, B. (2000) Siloxane polymers for high-resolution, high-accuracy soft lithography. *Macromolecules* **33**, 3042–3049.
82. Falconnet, D., Pasqui, D., Park, S., Eckert, R., Schift, H., Gobrecht, J., Barbucci, R., and Textor, M. (2004) A novel approach to produce protein nanopatterns by combining nanoimprint lithography and molecular self-assembly. *Nano Lett*. **4**, 1909–1914.
83. Hoff, J. D., Cheng, L. J., Meyhofer, E., Guo, L. J., and Hunt, A. J. (2004) Nanoscale protein patterning by imprint lithography. *Nano Lett*. **4**, 853–857.
84. Zhu, X. Y., Mills, K. L., Peters, P. R., Bahng, J. H., Liu, E. H., Shim, J., Naruse, K., Csete, M. E., et al. (2005) Fabrication of reconfigurable protein matrices by cracking. *Nat. Mater.* **4**, 403–406.
85. Suh, K. Y., Khademhosseini, A., Jon, S., and Langer, R. (2006) Direct confinement of individual viruses within polyethylene glycol (PEG) nanowells. *Nano Lett*. **6**, 1196–1201.
86. Khademhosseini, A., Jon, S., Suh, K. Y., Tran, T. N. T., Eng, G., Yeh, J., Seong, J., and Langer, R. (2003) Direct patterning of protein- and cell-resistant polymeric monolayers and microstructures. *Adv. Mater.* **15**, 1995–2000.
87. Khademhosseini, A., Suh, K. Y., Yang, J. M., Eng, G., Yeh, J., Levenberg, S., and Langer, R. (2004) Layer-by-layer deposition of hyaluronic acid and poly-L-lysine for patterned cell co-cultures. *Biomaterials* **25**, 3583–3592.
88. Suh, K. Y., Khademhosseini, A., Yang, J. M., Eng, G., and Langer, R. (2004) Soft lithographic patterning of hyaluronic acid on hydrophilic substrates using molding and printing. *Adv. Mater.* **16**, 584–588.
89. Suh, K. Y., Seong, J., Khademhosseini, A., Laibinis, P. E., and Langer, R. (2004) A simple soft lithographic route to fabrication of poly(ethylene glycol) microstructures for protein and cell patterning. *Biomaterials* **25**, 557–563.
90. Yang, T. L., Baryshnikova, O. K., Mao, H. B., Holden, M. A., and Cremer, P. S. (2003) Investigations of bivalent antibody binding on fluid-supported phospholipid membranes: the effect of hapten density. *J. Am. Chem. Soc*. **125**, 4779–4784.
91. Groves, J. T. and Dustin, M. L. (2003) Supported planar bilayers in studies on immune cell adhesion and communication. *J. Immunol. Methods* **278**, 19–32.
92. Sackmann, E. and Tanaka, M. (2000) Supported membranes on soft polymer cushions: fabrication, characterization and applications. *Trends Biotechnol*. **18**, 58–64.

Q9

93. Christensen, S. M. and Stamou, D. (2007) Surface-based lipid vesicle reactor systems: fabrication and applications. *Soft Matter* **3**, 828–836.

94. Groves, J. T., Ulman, N. and Boxer, S. G. (1997) Micropatterning fluid lipid bilayers on solid supports. *Science* **275**, 651–653.

95. Yee, C. K., Amweg, M. L., and Parikh, A. N. (2004) Membrane photolithography: direct micropatterning and manipulation of fluid phospholipid membranes in the aqueous phase using deep-UV light. *Adv. Mater.* **16**, 1184–1189. Q10

96. Yu, C. H., Parikh, A. N., and Groves, J. T. (2005) Direct patterning of membrane-derivatized colloids using in-situ UV-ozone photolithography. *Adv. Mater.* **17**, 1477–1480.

97. Orth, R. N., Kameoka, J., Zipfel, W. R., Ilic, B., Webb, W. W., Clark, T. G., and Craighead, H. G. (2003) Creating biological membranes on the micron scale: forming patterned lipid bilayers using a polymer lift-off technique. *Biophys. J.* **85**, 3066–3073.

98. Orth, R. N., Wu, M., Holowka, D. A., Craighead, H. G., and Baird, B. A. (2003) Mast cell activation on patterned lipid bilayers of subcellular dimensions. *Langmuir* **19**, 1599–1605.

99. Wu, M., Holowka, D., Craighead, H. G., and Baird, B. (2004) Visualization of plasma membrane compartmentalization with patterned lipid bilayers. *Proc. Natl. Acad. Sci. USA* **101**, 13798–13803.

100. Moran-Mirabal, J. M., Edel, J. B., Meyer, G. D., Throckmorton, D., Singh, A. K., and Craighead, H. G. (2005) Micrometer-sized supported lipid bilayer arrays for bacterial toxin binding studies through total internal reflection fluorescence microscopy. *Biophys. J.* **89**, 296–305.

101. Groves, J. T. and Boxer, S. G. (2002) Micropattern formation in supported lipid membranes. *Acc. Chem. Res.* **35**, 149–157.

102. Lenz, P., Ajo-Franklin, C. M., and Boxer, S. G. (2004) Patterned supported lipid bilayers and monolayers on poly(dimethylsiloxane). *Langmuir* **20**, 11092–11099.

103. Vidic, J., Pla-Roca, M., Grosclaude, J., Persuy, M. A., Monnerie, R., Caballero, D., Errachid, A., Hou, Y. X., et al. (2007) Gold surface functionalization and patterning for specific immobilization of olfactory receptors carried by nanosomes. *Anal. Chem.* **79**, 3280–3290.

104. Kam, L. and Boxer, S. G. (2000) Formation of supported lipid bilayer composition arrays by controlled mixing and surface capture. *J. Am. Chem. Soc.* **122**, 12901–12902.

105. Schuy, S. and Janshoff, A. (2006) Structuring of phospholipid bilayers on gold surfaces by micromolding in capillaries. *J. Colloid Interface Sci.* **295**, 93–99.

106. Yang, T. L., Jung, S. Y., Mao, H. B., and Cremer, P. S. (2001) Fabrication of phospholipid bilayer-coated microchannels for on-chip immunoassays. *Anal. Chem.* **73**, 165–169.

107. Kam, L. and Boxer, S. G. (2003) Spatially selective manipulation of supported lipid bilayers by laminar flow: steps toward biomembrane microfluidics. *Langmuir* **19**, 1624–1631.

108. Kim, P., Lee, S. E., Jung, H. S., Lee, H. Y., Kawai, T., and Suh, K. Y. (2006) Soft lithographic patterning of supported lipid bilayers onto a surface and inside microfluidic channels. *Lab Chip* **6**, 54–59.

109. Jiang, F. Z., Khairy, K., Poole, K., Howard, J., and Muller, D. J. (2004) Creating nanoscopic collagen matrices using atomic force microscopy. *Microsc. Res. Tech.* **64**, 435–440.

110. Wilson, D. L., Martin, R., Hong, S., Cronin-Golomb, M., Mirkin, C. A., and Kaplan, D. L. (2001) Surface organization and nanopatterning of collagen by dip-pen nanolithography. *Proc. Natl. Acad. Sci. USA* **98**, 13660–13664.

111. Zhang, G. J., Tanii, T., Zako, T., Hosaka, T., Miyake, T., Kanari, Y., Funatsu, T. W., and Ohdomari, I. (2005) Nanoscale patterning of protein using electron beam lithography of organosilane self-assembled monolayers. *Small* **1**, 833–837.

112. Cherniavskaya, O., Chen, C. J., Heller, E., Sun, E., Provezano, J., Kam, L., Hone, J., Sheetz, M. P., et al. (2005) Fabrication and surface chemistry of nanoscale bioarrays designed for the study of cytoskeletal protein binding interactions and their effect on cell motility. *J. Vac. Sci. Technol. B* **23**, 2972–2978.

113. Lussi, J. W., Tang, C., Kuenzi, P. A., Staufer, U., Csucs, G., Voros, J., Danuser, G., Hubbell, J. A., et al. (2005) Selective molecular assembly patterning at the nanoscale: a novel platform for producing protein patterns by electron-beam lithography on SiO2/indium tin oxide-coated glass substrates. *Nanotechnology* **16**, 1781–1786.

114. Kim, P., Kim, D. H., Kim, B., Choi, S. K., Lee, S. H., Khademhosseini, A., Langer, R., and Suh, K. Y. (2005) Fabrication of nanostructures of polyethylene glycol for applications to protein adsorption and cell adhesion. *Nanotechnology* **16**, 2420–2426.

115. Cheng, L. J., Kao, M. T., Meyhofer, E., and Guo, L. J. (2005) Highly efficient guiding of microtubule transport with imprinted CYTOP nanotracks. *Small* **1**, 409–414.

116. Cai, Y. G. and Ocko, B. M. (2005) Large-scale fabrication of protein nanoarrays based on nanosphere lithography. *Langmuir* **21**, 9274–9279.

117. Michel, R., Reviakine, I., Sutherland, D., Fokas, C., Csucs, G., Danuser, G., Spencer, N. D., and Textor, M. (2002) A novel approach to produce biologically relevant chemical patterns at the nanometer scale: selective molecular assembly patterning combined with colloidal lithography. *Langmuir* **18**, 8580–8586.

118. Michel, R., Lussi, J. W., Csucs, G., Reviakine, I., Danuser, G., Ketterer, B., Hubbell, J. A., Textor, M., et al. (2002) Selective molecular assembly patterning: a new approach to micro- and nanochemical patterning of surfaces for biological applications. *Langmuir* **18**, 3281–3287.

119. Karuri, N., Liliensiek, S., Teixeira, A., Abrams, G., Campbell, S., Nealey, P., and Murphy, C. (2004) Biological length scale topography enhances cell-substratum adhesion of human corneal epithelial cells. *J. Cell Sci.* **117**, 3153–3164.

120. Kim, D., Kim, P., Song, I., Cha, J., Lee, S., Kim, B., and Suh, K. Y. (2006) Guided three-dimensional growth of functional cardiomyocytes on polyethylene glycol nanostructures. *Langmuir* **22**, 5419–5426.

121. Suh, K. Y. and Jon, S. (2005) Control over wettability of polyethylene glycol surfaces using capillary lithography. *Langmuir* **21**, 6836–6841.

122. Charest, J., Eliason, M., Garcia, A., and King, W. (2006) Combined microscale mechanical ttopography and chemical patterns on polymer cell culture substrates. *Biomaterials* **27**, 2487–2494.

123. Rajnicek, A. M., Britland, S., and McCaig, C. D. (1997) Contact guidance of CNS neurites on grooved quartz: influence of groove dimensions, neuronal age and cell type. *J. Cell Sci.* **110**, 2905–2913.

124. Oakley, C. and Brunette, D. M. (1993) The sequence of alignment of microtubules, focal contacts and actin-filaments in fibroblasts spreading on smooth and grooved titanium substrata. *J. Cell Sci.* **106**, 343–354.

125. Teixeira, A. I., Abrams, G. A., Bertics, P. J., Murphy, C. J., and Nealey, P. F. (2003) Epithelial contact guidance on well-defined micro- and nanostructured substrates. *J. Cell Sci.* **116**, 1881–1892.

126. Teixeira, A. I., McKie, G. A., Foley, J. D., Bertics, P. J., Nealey, P. F., and Murphy, C. J. (2006) The effect of environmental factors on the response of human corneal epithelial cells to nanoscale substrate topography. *Biomaterials* **27**, 3945–3954.

LIST OF QUERY

Q1. Please check phrase “low aseptic ratio” here. Do you mean “low aspect ratio”? Please confirm.

Q2. Please expand ”SDS” here.

Q3. Please expand “BSA” here.

Q4. Please check whether the expanded form of AFM is OK as supplied.

Q5. We have changed phrase “(PUA)-functionalized polyurethane” to “poly(urethaneacrylate) (PUA)-functionalized polyurethane.” Could you please confirm that it is OK?

Q6. We have located the names of the authors on Goggle and supplied to reference [15]. Could you please confirm that the names are OK?

Q7. Please check the supplied page range as well as the change made in the first name and surname of the authors in reference [21].

Q8. Please check the supplied volume number.

Q9. Please check the supplied page range in reference [88].

Q10. Please check the supplied page range in reference [95].

Q11. In Artwork 13.12, we have deleted subpart label (c) under part (B). Could you please confirm that it is OK? (Part (B) has been changed to (*b*) and its subparts have been changed to (1) and (2) for stylistic reasons.)